DIMENSIONAL STUDY OF AN INTERFERENCE FIT ALLOGRAFT

By

NATHAN A. MAUNTLER

A THESIS PRESENTED TO THE GRADUATE SCHOOL
OF THE UNIVERSITY OF FLORIDA IN PARTIAL FULFILLMENT
OF THE REQUIREMENTS FOR THE DEGREE OF
MASTER OF SCIENCE

UNIVERSITY OF FLORIDA

2006

This thesis is dedicated to my mother, Margaret Mauntler: the most selfless, dedicated, and loving person I know. Thank you for your love, your support, your faith, and all those cookies you sent from Ohio.

ACKNOWLEDGMENTS

I would first like to thank my graduate committee Tony L. Schmitz (chair), W. Gregory Sawyer, and John C. Ziegert for their guidance, their support, and their patience. I would like to thank the members of the Tribology Laboratory and the Machine Tool Research Center at the University of Florida: Jerry Bourne, Dave Burris, Matt Hamilton, Luis Alvarez, Alison Dunn, Pam and Dan Dickrell, Vince Lee, Nick Argibay, Chris Martens, Kevin Powell, Scott Payne, G. Scott Duncan, Raul Zapata, Lee Kumanchik, Kevin Cheng, and Lonny Houck. I am very grateful for their friendship, their comradeship, their help, and their shenanigans.

I wish to thank Becky Bassett, Earl Jones, Roy Clark, Jason Bootle, and the rest of the staff at Regeneration Technologies, Inc. for their generous support and access to their facilities. Finally, I would like to acknowledge the generosity and kindness of the donors who make the fine work at Regeneration Technologies possible.

TABLE OF CONTENTS

LIST OF TABLES

LIST OF FIGURES

Abstract of Thesis Presented to the Graduate School
of the University of Florida in Partial Fulfillment of the
Requirements for the Degree of Master of Science

DIMENSIONAL STUDY OF AN INTERFERENCE FIT ALLOGRAFT

By

Nathan A. Mauntler

August 2006

Chair: Tony L. Schmitz
Major Department: Mechanical and Aerospace Engineering

The Cornerstone™ ASR cortical-cancellous allograft made by Regeneration Technologies, Inc. (RTI) of Alachua, Florida, is an implant used in cervical spinal fusion surgeries. Making use of two cortical bone plates for structural support surrounding a cancellous bone block for growth conduction, the graft is held together by two cortical interference pins. The success of the interference fit depends on the manufacturing tolerances of the components as well as the quality of the donor bone used to produce the graft.

In this study, the diameters of interference pins and cortical plate holes required to produce thirty allografts are measured on a coordinate measuring machine at four critical points in the manufacturing cycle: after machining, after chemical sterilization, after freeze-drying (lyophilization), and after re-hydration. A statistical distribution of the interference fit component dimensions is obtained. Lyophilization is found to have the largest effect on the component dimensions, causing an average decrease of 21 μm in the predicted interference, which should nominally be between 25 and 38 μm.

Thirty separate allografts are manufactured by RTI to investigate the occurrence of pull-apart failure and cracking in the allografts. Of the thirty grafts, seventeen (57%) showed signs of cracking on one or both of the cortical plates. Four (13%) of the grafts failed manual pull-apart tests following lyophilization and prior to hydration. Following a thirty second hydration, the grafts were epoxied to aluminum plates and pulled apart on a mechanical tensile testing machine. For twenty of the grafts, one plate was removed from the interference fit at an average pull-apart force of 83.4 N. For the remaining ten grafts, the epoxy failed prior to interference fit failure. Of the seven grafts that were separated and showed no signs of cracking, the average pull-apart force was found to be 100.6 N. Any relationship between the predicted diametric interference value and the pull-apart force was obscured by the small sample size of undamaged grafts and variations in material property.

A finite element analysis of the interference fit is created to attempt to model the scenario observed in the mechanical testing. The model predicts a pull-apart force of 93 N and a maximum von Mises stress of 35 MPa. Additionally, the model shows no evidence of a stress concentration at the edge of the contact.

Finally, a Monte Carlo simulation based on an isotropic analytical model of the interference fit is developed. In this simulation, the input parameters are varied by random values within one standard deviation of the mean. The Monte Carlo simulation indicates that diametric interference is the largest factor affecting the interference fit. The simulation accurately predicts the rate of occurrence of pull-apart and material failures at 13% and 57%, respectively.

CHAPTER 1
INTRODUCTION AND PROBLEM STATEMENT

This thesis describes an investigation of an interference-fit allograft used in spinal fusion surgeries. Spinal fusion is the joining of two vertebrae in order to treat degenerative disk disease or otherwise remove pressure from the spinal cord. Fusion is accomplished by inserting a graft between the two vertebrae. This graft serves both as a structural support and a medium through which the two bones can grow together and eventually fuse. Grafts made from human cadaver bone are known as allografts.

One such allograft is the Cornerstone™ ASR cortical-cancellous block manufactured by Regeneration Technologies, Inc. (RTI) for use in cervical spine fusion surgeries (Figure 1-1). This graft is assembled from a cancellous bone block sandwiched between two cortical bone plates held together by two interference-fit pins. The cortical plates provide structural strength while the cancellous block provides a medium for new bone growth. By manufacturing the graft from separate cortical and cancellous pieces, more efficient use can be made of the bone donor material. Also, the use of an interference connection for the assembly enables an all-bone construction.

Drawbacks to an interference fit connection include the possibility of pull-apart failure and cracking. Pull-apart failure occurs when the strength of the interference fit is insufficient to hold the graft together under tensile loads (Figure 1-2). Pull-apart failure can occur as a result of inadequate radial interference (the pin is insufficiently larger than the plate holes) or as a result of the components having too much mechanical compliance. Cracking occurs when the stresses caused by the interference fit are large enough to cause

material failure in the bone. As opposed to pull-apart failure, cracking is the result the radial interference or material stiffness being too large.

The purpose of this study is to examine the quality of the ASR interference fit connection in the light of the various RTI manufacturing processes in order to identify the most probably failure source. To this end, dimensional measurements of the pins and cortical plate holes and mechanical pull-apart tests are performed to characterize the accuracy of the RTI machining process and the effects of various chemical, dehydration, and re-hydration treatments. Mechanical testing is used to measure the force required to separate the interference fit. Finally, a finite element analysis of the graft and a Monte Carlo simulation are performed to predict interference fit failures.

Dimensional Measurements and Mechanical Testing

In the dimensional study, the diameters of pins and cortical plate holes are measured at various points throughout the manufacturing process. The parts required to produce six grafts from each of ten donors are provided by RTI. Half of these grafts follow the normal manufacturing cycle/assembly steps in order to later measure the force required to separate the interference fit. The remaining pieces are not assembled so that dimensional measurements may be performed. Pin and hole diameter measurements are recorded after each of the following manufacturing processes:

- Machining
- The chemical sterilization process BioCleanse™
- Freeze-drying, or lyophilization
- Hydration for thirty seconds.

Modeling

The data obtained from the dimensional measurements are then used along with published material properties to create a finite element model of the interference fit. This

three-dimensional orthotropic model is used to simulate the stresses and pressures present in the allograft as well as the pull-apart force. The finite element model is in turn used to validate and improve an isotropic analytical model which was used in a Monte Carlo simulation, a computational technique where the model inputs are randomly selected from pre-selected distributions and used to compute the output over many iterations. The results of the Monte Carlo simulation is a statistical distribution of the output parameters (e.g. stress, pressure, and pull-apart force). Finally, the stresses and pull-apart forces predicted by the finite element model and Monte Carlo analysis are compared to the failures observed in the actual allografts.

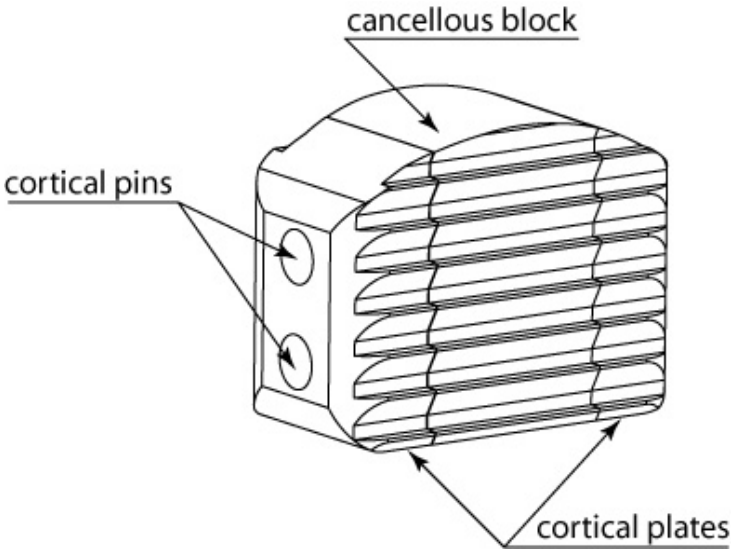

Figure 1-1. The Cornerstone™ ASR cortical-cancellous allograft

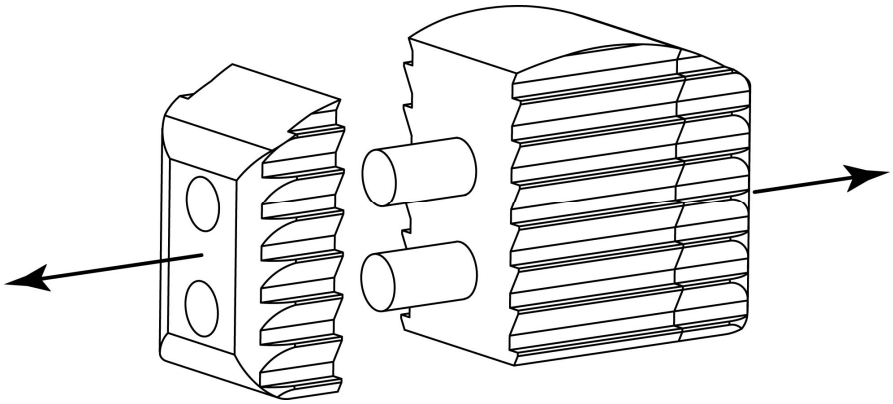

Figure 1-2. Allograft failure by pull-apart.

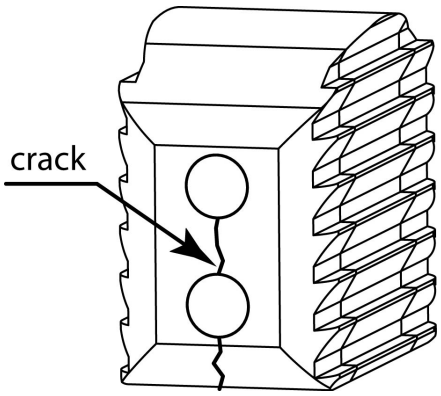

Figure 1-3. Stress cracking in an allograft plate.

CHAPTER 2
REVIEW OF THE LITERATURE

To make predictions regarding the effectiveness of the allograft interference connections, it is necessary to have an understanding of the mechanical behavior of bone from an engineering standpoint. Once the physical properties of bone are identified, they can be applied to mechanical models which simulate the conditions of the interference fit. The following sections provide a review of publications relevant to the study of bone as an engineering material and its application to specific mechanical scenarios. A discussion of relevant analytical and finite element modeling techniques is also included.

The Structure and Mechanical Properties of Bone

Bone is a composite material comprised of an inorganic phase, primarily hydroxyapatite ($Ca_{10}(PO)_4)_6(OH)_2$) crystals, embedded in an organic matrix, primarily collagen.[1] At the micrometer level, these collagen fibrils and embedded hydroxyapatite crystals bundle to form fibers.[2] The organization of these bone fibers above the micrometer level depends on the development and function of the bone area of interest.[3]

Classifications of Developed Bone

The macrostructure of mature bone can be categorized as cortical or cancellous. Slow-forming cortical, or compact, bone is made up of organized layers, or lamellae, which form in nominally parallel cylindrical patterns.[2] The directionality of these lamellae causes cortical bone to have anisotropic properties. Strictly speaking, the elastic properties of cortical bone are orthotropic. However, little error is introduced by modeling cortical bone material from long bones as transversely isotropic in nature.[4] In

long bones such as the femur and tibia, cortical bone forms in the central shaft, or diaphyis.[6]

In contrast, cancellous, or trabecular, material is made up of a porous matrix of bony struts, called trabeculae, packed with mineral and marrow deposits.[1,2] In general, the bulk properties of cancellous bone are functions of the density and directionality of this matrix.[3] In long bones, cancellous material primarily forms on the ends (epiphyses) of the bones, but can also be found under the cancellous surface of the shaft close to the epiphyses.[3,5] The transition within a bone from cancellous to cortical material can be gradual and microstructural analysis is often necessary to distinguish between the two.[2]

Assigning values to the material properties of bone material, whether cortical or cancellous, is not trivial. Factors that can affect the elastic and strength properties include mineral content, trabecular density, the type of bone, the harvest location on the donor bone, and the scale at which measurements are taken.[1-3,6-11] To try to address these issues, a wide variety of methods have been used to investigate bone mechanics. Buckling tests, tension tests, compression tests, bending tests, indentation methods, acoustic methods, and x-ray computed tomography have all been used to measure the elastic and failure properties of cortical and cancellous bone.[3,12-15] For the sake of relevance and to limit the discussion to a reasonable length, the following subsections are limited to a discussion of human femoral and tibial bone only.

Mechanical Properties of Cortical Femoral and Tibial Bone Material

Table 2-1 contains data compiled by Cowin[1] and Currey[3] from mechanical and ultrasound studies of the elastic properties of cortical bone material.[16-19] Data from Reilly and Burstein suggests that cortical bone can behave differently in tension than in compression.[16-17] Standard deviations, where applicable, are in parentheses. Note that

two of these studies assume transversely isotropic material symmetry while the other two account for orthotropic material properties. Here, the "1" direction corresponds to the radial bone direction, the "2" direction corresponds to the circumferential bone direction, and the "3" direction corresponds to the radial bone direction. It should be noted that the values for Poisson's ratio greater than 0.5 reported by Reilly and Burstein are physically impossible.

Table 2-2 contains a collection of material strength information for cortical bone under a variety of loading conditions and physical treatments relevant to this study.[5] This data is of particular interest since it represents RTI donor material for use in spinal allografts. Note that the standard deviation of the failure stress is between 12% and 25% of the mean value. This gives some indication of the substantial variation in material properties that can be present from sample to sample for bone material. For comparison, Reilly and Burstein report the tensile strength of bone as 53 MPa in the circumferential direction and 133 MPa in the longitudinal direction and the compressive strength of bone as bone 131 MPa in the circumferential direction and 205 MPa in the longitudinal direction.[16]

Mechanical Properties of Cancellous Material

While cancellous bone is, strictly speaking, orthotropic, for practical purposes it is becoming common to model cancellous bone as isotropic.[6,20] While values for the elastic modulus of trabeculae are on par with those of cortical bone,[3] Young's modulus values for bulk cancellous material is substantially smaller. Rice et al. suggest that both Young's modulus and the cancellous bone strength are dependent on the apparent density of the material to the second power.[21] The same study reported values all less than 500 MPa for the bulk Young's modulus of human cancellous bone. Since the modulus values

for bulk cancellous bone are so much smaller than those of cortical bone, the effect of cancellous bone is neglected in the following analyses.

Analytical Interference Fit Models

Once the mechanical properties of bone material are understood, they can be incorporated into specific mechanical models. The classic analytical model of an interference fit connection is the hollow, thick-walled cylinder representation shown in Figure 2-1.[22] In this model, a hollow cylinder "1" of nominal outer radius R is forced into another hollow cylinder "2" whose inner radius is some amount δ smaller than R. To accommodate the radial interference, both cylinders must deform such that the outer radius of cylinder "1" decreases by some amount δ1 while the inner radius of cylinder "2" increases by some amount δ2. The deformations δ1 and δ2 must add up to the radial mismatch δ.

Stress, Pressure, and Pull-apart Force Predictions

The two-dimensional state of stress at the boundary of either cylinder can be described in terms of the pressure p at the interface and the three radii as in Eq. (2-1) through Eq. (2-4). In these equations σ1t and σ2t represent the tangential stresses of cylinders 1 and 2 while σ1r and σ2r represent the radial stresses in cylinders 1 and 2. The sign convention is such that positive stresses are tensile and negative stresses are compressive. If the two cylinders are not both infinitely long, a stress concentration will exist at the edges of the contact. For this reason, the stress concentration factor Kt is included in the radial stress equations. A stress concentration factor of 2 is a reasonable upper bound value.[22]

$$\sigma 1t = -p \cdot \frac{R^2 + ri^2}{R^2 - ri^2} \tag{2-1}$$

$$\sigma 2t = p \cdot \frac{ro^2 + R^2}{ro^2 - R^2} \tag{2-2}$$

$$\sigma 1r = -Kt \cdot p \tag{2-3}$$

$$\sigma 2r = -Kt \cdot p \tag{2-4}$$

The von Mises equivalent stress σv at the interface of either cylinder can be calculated as shown in Eq. (2-5), where σ1 and σ2 represent the two-dimensional principal stresses. Substituting Eq. (2-1) through Eq. (2-4) into Eq. (2-5), the von Mises stresses for cylinder "1" in Eq. (2-6) and cylinder "2" in Eq.(2-7) can be found. Since in this study the pin (cylinder "1") is solid, ri is assigned a value of zero. The calculated von Mises stresses can then be directly compared to the failure strength of the cylinder materials.

$$\sigma v = \sqrt{\sigma 1^2 - \sigma 1 \cdot \sigma 2 + \sigma 2^2} \tag{2-5}$$

$$\sigma v1 = p \cdot \sqrt{Kt^2 - Kt + 1} \tag{2-6}$$

$$\sigma v2 = p \cdot \sqrt{Kt^2 + Kt \cdot \left(\frac{ro^2 + R^2}{ro^2 - R^2} \right) + \left(\frac{ro^2 + R^2}{ro^2 - R^2} \right)^2} \tag{2-7}$$

Thick-walled cylinder elastic theory can be used to calculate the pressure p at the press-fit interface as in Eq. (2-8), where E represents Young's modulus and υ represents Poisson's ratio. The force required to separate the interference fit can be found from Eq. (2-9) where Ac represents the area in contact, Lc represents the length of the contact and μ represents the static coefficient of friction between the inner pin and outer plate. If Eq.

(2-1) through Eq. (2-9) are assumed to provide a reasonable representation of an interference fit, the force required to separate a cortical plate from two cortical pins could be estimated by multiplying the force F in Eq. (2-9) by a factor of two. The integral in equation 2-9 is to account for the fact that the stress concentration factor is not constant along the length of the contact, designated here as the x-direction.

$$p = \frac{\delta}{\frac{R}{E1}\cdot(1-\nu 1)+\frac{R}{E2}\cdot\left(\frac{ro^2+R^2}{ro^2-R^2}+\nu 2\right)} \tag{2-8}$$

$$F = \int Kt(x)\cdot p\cdot(Ac)\cdot\mu\, dx = \int Kt(x)\cdot p\cdot(2\cdot\pi\cdot R\cdot Lc)\cdot\mu\, dx \tag{2-9}$$

Limitations of the Analytical Model

The analytical model has three primary limitations. First, the assumption is made that the material properties of both the pin and plate are isotropic in nature. Secondly, this model cannot account for the effect a second pin in close proximity would have on the stress state. Finally, the model cannot account for plate geometry that is not cylindrical.

Finite Element Analysis of Bone

Due to the limitations of analytical models, finite element analysis has become a common method of modeling bone behavior. The following paragraphs discuss several application of the finite element method to various scenarios involving bone.

The choice of a finite element model depends on the geometric and mechanical complexity of the scenario being modeled. Often, three-dimensional models are necessary, but under certain circumstances, simplifying assumptions can be applied to reduce the computational requirements. Plane strain, plane stress conditions, or

axisymmetric conditions can justify the use of two-dimensional models. Two- or three-dimensional models can also be simplified when loads, boundary conditions, and material properties are symmetric about a given axis.

When modeling the reconstruction of mandibles, Nagasao et al. and Tie et al. used computed tomography (CT) scans to create solid models with accurate information regarding the location and thickness of cortical and cancellous bone.[23-25] Nagasao et al. used 10-node tetrahedral elements for the entire model while Tie et al used four-node tetrahedral elements to model the cancellous inner mandible and membrane shell elements to model the thin cortical shell. Both studies assumed isotropic material properties; see Table 2-3.

Similarly, Barker et al. used CT scans to create a three-dimensional model of a human metacarpal.[26] Additionally, bone density information from the CT scans was used to predict calcium and potassium content. Power laws developed by Lotz et al. and Dalstra et al. were then used to create isotropic and orthotropic material models.[12,13] The solid models were meshed using hexahedral and pentahedral elements without mid-side nodes.

Wang and Dumas used 8-node brick elements with isotropic material properties for both cortical and cancellous spinal bone when modeling an inter-vertebral fusion scenario.[27] This study investigated the likely variation in material properties from bone to bone by using a range of values for both Young's modulus and Poisson's ratio (Table 2.4).

When studying stress concentration created by surgically drilled holes in canine tibia, Zapata used a two-dimensional axisymetric model.[28] Transversely isotropic

material properties were used to model the cortical tibial bone while isotropic material properties were used to model woven bone growing where the hole was drilled. The model was meshed using quadrilateral elements.

In this study, we will apply a three-dimensional model solid model of one cortical plate and two cortical pins. The model is meshed with 20-node orthotropic hexahedral elements. Transversely isotropic material properties are used for both the cortical plate and the cortical pins.

Table 2-1. A survey of the elastic properties of cortical bone compiled by.

	Reilly and Burstein (1975) [16]		Yoon and Katz (1976) [17]	Knets et al. (1977) [18]	Ashman et al. (1984) [19]
	Compression	Tension			
Symmetry applied	Transversely Isotropic	Transversely Isotropic	Transversely Isotropic	Orthotropic	Orthotropic
Bone type	Femur	Femur	Femur	Tibia	Femur
Testing method	Mechanical	Mechanical	Ultrasound	Mechanical	Ultrasound
E1 (GPa)	11.5 (1.01)	12.8 (3.0)	18.8	6.91	12.0
E2 (GPa)	11.5 (1.01)	12.8 (3.0)	18.8	8.51	13.4
E3 (GPa)	18.2 (0.85)	17.7 (3.6)	27.4	18.4	20.0
G12 (GPa)	3.6	3.6	7.17	2.41	4.53
G13 (GPa)	3.3 (0.42)	3.3 (0.42)	8.71	3.56	5.61
G23 (GPa)	3.3 (0.42)	3.3 (0.42)	8.71	4.91	6.23
v12	0.63 (0.20)	0.53 (0.25)	0.312	0.49	0.376
v13	0.38 (0.15)	0.41 (0.15)	0.193	0.12	0.222
v23	0.38 (0.15)	0.41 (0.15)	0.193	0.14	0.235
v21	0.63 (0.20)	0.53 (0.25)	0.312	0.63	0.422
v31	0.38 (0.15)	0.41 (0.15)	0.281	0.32	0.371
v32	0.38 (0.15)	0.41 (0.15)	0.281	0.31	0.35

[1,3]

Table 2-2. A study of RTI donor cortical bone strength.

Treatment	Axial Compression		Transverse Shear		Transverse Tension	
	Mean	St. Dev.	Mean	St. Dev.	Mean	St. Dev.
Physiologic	204	24.5	84.7	16.2	29	5.0
Freeze dried (FD)	303	75.9	60.3	15.0	31.8	10.1
FD + Reconstituted	169	19.6	97.0	13.8	24.7	5.3
BioCleanse™	203	36.1	-	-	29.2	4.6

[5]

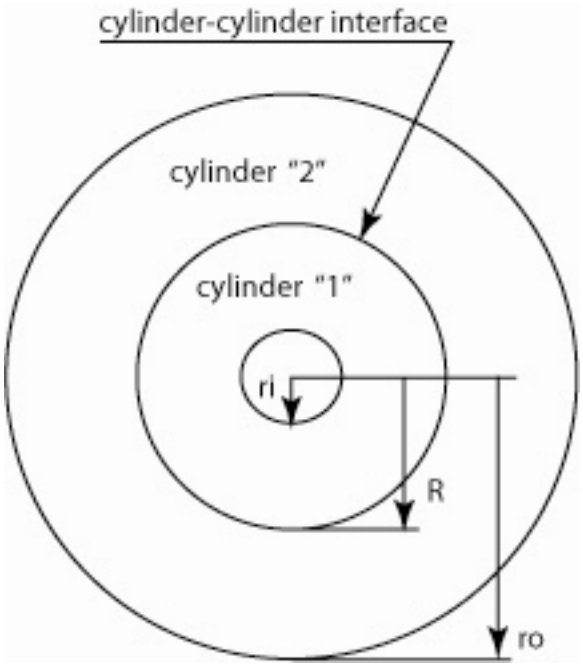

Figure 2-1. An analytical model of an interference fit between two cylinders.

Table 2-3. Bone elastic material properties used in finite element studies.

	Young's modulus (GPa)	Poisson's ratio
Cortical bone	15	0.33
Cancellous bone	1.5	0.3

[23-25]

Table 2-4. Bone elastic material properties used in study of an inter-vertebral fusion degeneration

CHAPTER 3
THE CORNERSTONE™ ASR ALLOGRAFT MANUFACTURING PROCESS

The ASR cervical spinal allograft is produced using femoral or tibial bone from a single donor. Donor material is processed from whole limbs which are received frozen. After removing the soft tissue, the bones are cut into blanks, machined to shape, assembled, cleaned, and freeze dried as discussed in the following sections. Each of the following sections occurs in a single machining episode to prevent the intermixing of donor material.

Cutting Blanks For Machining

The bones are cut into blanks using a stainless steel band saw. Cortical blanks are taken from the shaft (diaphysis) of the bones while cancellous blanks are cut from the heads (Figure 3-1). Blanks for cortical plates are harvested from the stronger central portion of the shaft.

The cortical region of the donor bone has a finite thickness, so the cortical blanks must be cut in a specific orientation with respect to the lay of the bone (Figure 3-2). Cancellous blanks are chosen from the densest regions of cancellous bone. All blanks are cut oversized to accommodate final machining. Cortical pin blanks are cut 25 mm long and 3-4 mm wide. Cortical plate blanks are cut 12.5-13 mm long and to a width of the operator's discretion. Cortical pin and plate blank thicknesses are driven by the thickness of the bone raw material. Cancellous blanks are cut to 11.3 mm by 11.3 mm by 4.5 mm.

Preparation for Assembly

Cortical pin blanks are turned down to pins on an OmniTurn GT-Jr CNC lathe. The pins are first turned using conventional tooling, then "reamed" by a tubular tool with a sharpened inner edge to a nominal diameter of 2 mm (Figure 3-3). The reaming tool is produced by drilling a hole through a conventional reamer. When turning the pins, isopropyl alcohol is used as a cutting fluid. The turned pin is then parted from the blank, leaving a chamfer on one end (Figure 3-4). The length of the parted pin is approximately 17.5 mm. After the pins have been machined, they are immersed in alcohol, removed and left to dry for 15 minutes. They are then weighed to ensure that they meet minimum bone density requirements. The pins are finally sorted into groups with diameters in a 0.013 mm (0.0005 in) range.

Cortical plate blanks are squared on a Fadal 904-1L CNC mill. Blanks are first faced and squared on three sides in one clamp pallet, then faced and squared on the other three sides in a second clamp pallet. Like the cortical pins, the plates are checked for minimum mass requirements.

Cancellous blanks are dimineralized in 0.5 N HCL for 3-5 minutes, then submerged in water for 8-10 minutes. No further machining is required for the cancellous blanks.

Assembly and Finishing Cuts

Cortical plates and cancellous blocks are clamped in the assembling and grooving fixture (Figure 3-5). Six of these fixtures are then bolted into an indexing wheel. Two holes are drilled and reamed through the cortical-cancellous stack-ups. The diameter of the reamer is designated to be 0.025-0.038 mm (0.0010-0.0015 in) smaller than the pins which will be used for that graft. Isopropyl alcohol is used as a cutting fluid while reaming the holes.

Pins are inserted chamfered end first into the reamed holes using a custom tool (Figure 3-6). The side clamps of the machining fixture are then removed and the sides of the allograft are grooved. The interference fit assembly is then removed from the assembly and grooving fixture and loaded into the profiling fixture for final radius cuts. Allografts are then inspected and frozen.

BioCleanse™ Sterilization Process

BioCleanse™ is a chemical treatment that kills viral, fungal, and bacterial contaminants without adversely affecting the bone material properties.[30] Normally, a BioCleanse™ cycle is completed with allografts from a single donor. However, due to cost considerations, all donor material for this study was processed in a single BioCleanse™ batch. RTI offers BioCleanse™ in two different recipes depending on whether or not the donor material contains soft tissue. The more chemically aggressive hard-tissue-only recipe was used for this study since it was assumed to be more likely to adversely affect the material and dimensional properties of the allografts. Normally allografts are visually inspected, packaged, and stored frozen after completing the BioCleanse™ cycle. However, for this study, loose cortical plates and cortical pins were packaged in sealed plastic pouches and sent to the University of Florida for additional dimensional measurements (see Chapter 4).

Lyophilization Process

Lyophilization is a freeze drying process performed on allografts so that they may be stored at room temperature for extended periods. The allografts and allograft parts from donors 1-6 underwent lyophilization in one cycle while the material from donors 7-10 were run in a separate cycle.

After lyophilization, allografts are visually inspected for cracks and manually inspected for pull-apart failures. Since the pull-apart tests are performed by hand, the applied force is unknown. The allografts are then repackaged and the packages sterilized for distribution.

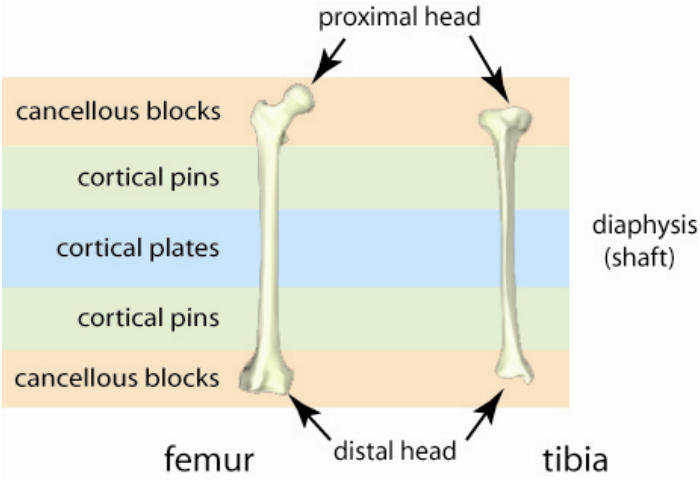

Figure 3-1. Cancellous blocks, cortical pins, and cortical plates are harvested from specific areas of the femur and tibia. Bone images from http://www.ana.cuhk.edu.hk/3dana/main.htm [29]

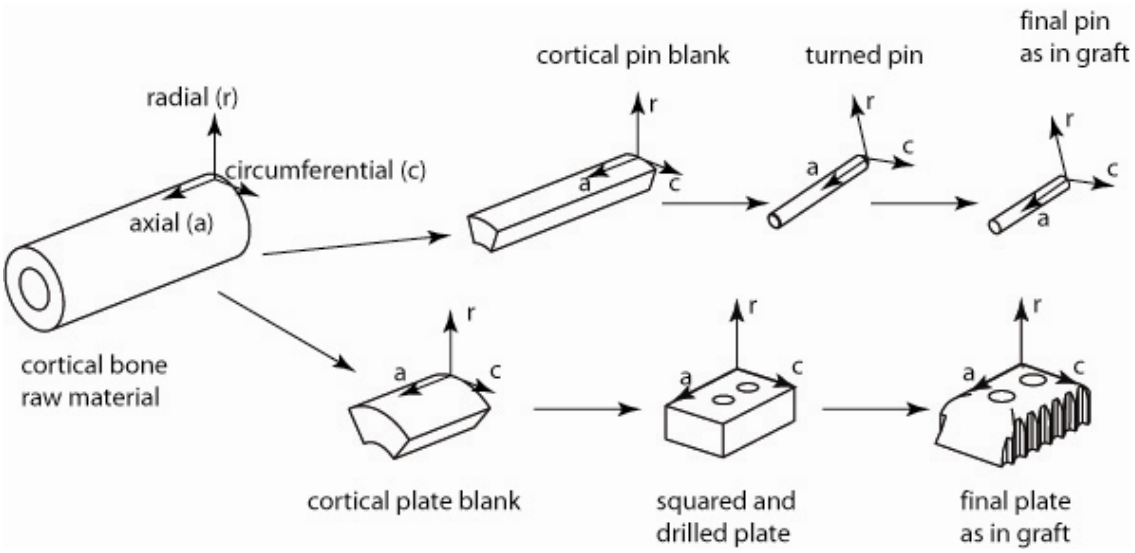

Figure 3-2. Orientation of the cortical bone pieces with respect to anatomical bone material directions.

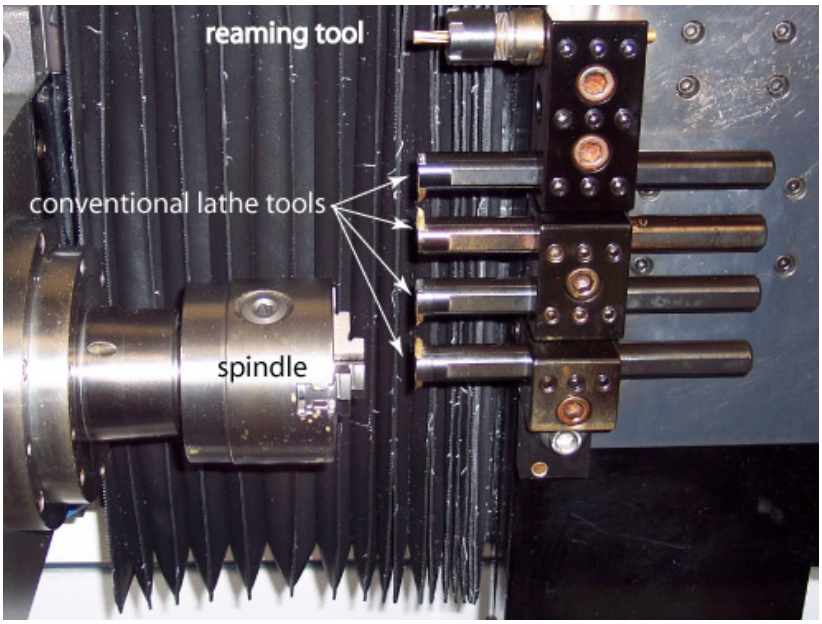

Figure 3-3. Lathe tooling for turning the cortical pins.

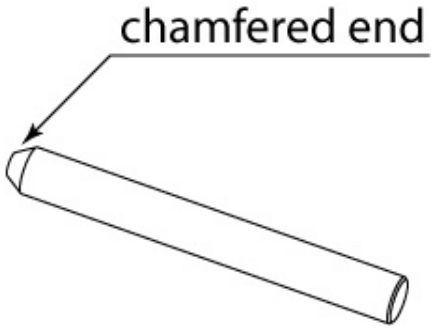

Figure 3-4. The chamfered end of a cortical pin.

Figure 3-5. Assembling and grooving fixture.

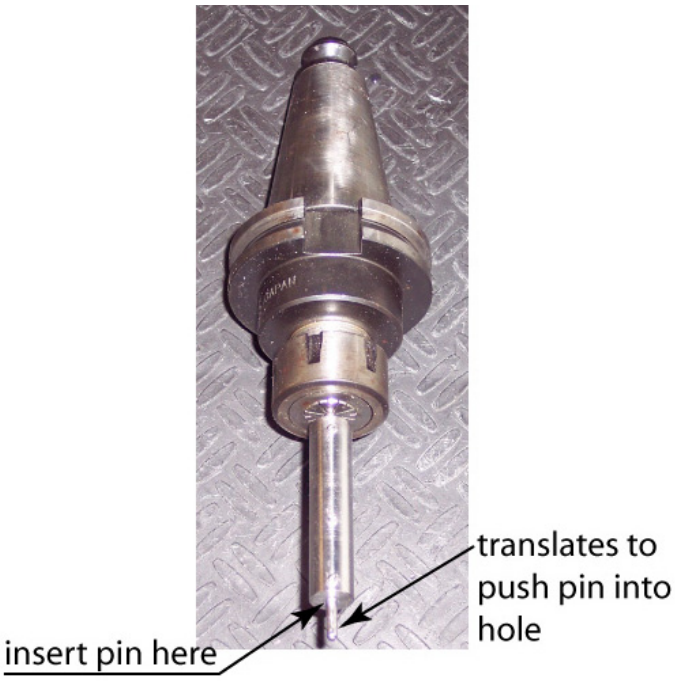

Figure 3-6. Custom tool for inserting interference pins into holes reamed in allograft.

CHAPTER 4
EQUIPMENT AND PROCEDURES

This chapter discusses the procedures used in this study, including measurement techniques, analytical and finite element models, and mechanical testing.

Dimensional Measurements

Measurements of the allograft stack-ups and components were carried out on a Brown and Sharpe MicroVal™ PFx three-axis coordinate measuring machine (Figure 4-1) using a Renishaw MIP touch-trigger probe. This coordinate measuring machine (CMM) is operated via PC-DMIS CAD++ software and is certified to be accurate to 12 μm over its work volume according to American National Standard ASME B89.4.1-2001b.[31]

The CMM could be operated in either manual mode or direct computer control (DCC) mode. In manual mode, the CMM was controlled by the operator using a joystick. In DCC mode, the CMM was commanded by the machine controller. In this study, the manual operation mode was used to locate parts and define the part coordinate frame. DCC mode was used to refine the alignment and take measurements.

Probe Tip Qualification

Two types of stylus probe tips were used in this study. A 20 mm long tip was used to measure the loose cortical plates and pins while a 27 mm long tip was used to measure the stack-ups held in the RTI assembly and grooving fixture. Both tips were composed of a 1 mm diameter ruby ball fixed to a carbide shank and steel body (Figure 4-2). Points were recorded by moving the CMM axes until the ruby ball came into contact with the

part being measured. This caused the probe tip to swivel within the probe housing until a switch registered the contact. A contact force of 0.1 N was required to register probe tip contact.

To ensure accurate measurements, the probe tips must be calibrated periodically. For this study, probe tips were calibrated if:

- The CMM controller had been turned off after the most recent calibration.
- The PC-DMIS software had been closed after the most recent calibration.
- The tip had not been calibrated for the current donor and measurement type.

The tip was qualified by taking 24 points about a spherical artifact. The diameter of this construct was then compared to the known 19.050 mm diameter of the artifact. Additionally, the standard deviation of the 24 radius values was calculated. The calibration was considered acceptable if the constructed diameter was accurate to better than 3 μm. A standard deviation of the radii of less than 2 μm was considered acceptable for the 20 mm long tip while a standard deviation of less than 4 μm was considered acceptable for the 27 mm long tip.

Measuring the Allograft Stack-ups and Parts

Dimensional measurements of the allograft pin and hole diameters were taken at four points during the manufacturing cycle: just prior to pin insertion, after BioCleanse™, after lyophilization, and after a 30 second hydration by immersion in water. A discussion of the RTI manufacturing procedure can be found in Chapter 3.

Grafts from ten donors were followed through the manufacturing process. Each donor set consisted of the parts required to make six allograft assemblies (Figure 4-3). The parts were first received prior to pin insertion with cortical plates and cancellous blocks still clamped in the RTI indexing wheel (Figure 4-4). At this time the holes in the

top cortical plate were measured. Half of the cortical-cancellous stack-ups were then removed so that individual cortical plates could be measured. The remaining three stack-ups were left in their respective machining fixtures and returned to RTI for final assembly and machining. This was done so that half the parts could be passed through the RTI manufacturing process for further measurements and half could be assembled for failure testing.

During this first measurement cycle, the twelve cortical pins per donor were also measured and sorted according to size. Six pins were selected to be inserted into three allografts including the two largest and two smallest pins. These extreme diameter pins were deliberately mismatched with the extreme diameter holes in order to try to increase the likelihood of fracture and pull-apart failures. The three assembled grafts per donor were then assembled, machined and treated as per RTI specifications with BioCleanse™ and lyophilization.

The remaining six pins along with the cortical plates that were removed from the RTI assembling and grooving fixtures were then re-measured after each remaining portion of the manufacturing sequence. The cancellous blocks were assumed to have no effect on the performance of the graft (see Chapter 2). For this reason, the cancellous blocks that were removed from the machining fixtures were discarded.

Cortical-cancellous stack-ups

As noted, the six cortical-cancellous stack-ups per donor were measured while still clamped in the RTI machining fixture prior to pin insertion. Each stack-up was assigned a label “ASM X-Y” where the prefix “ASM” designated the parts as an assembly, X was the position of the graft in the RTI indexing wheel (1-6), and Y was the donor number (1-10). Due to the limited length of the probe tip, only the topmost cortical plate could be

measured in the fixture. The two holes were designated as “hole 1” and “hole 2” as shown in Figure 4-5.

The indexing wheel was received from RTI sealed in a plastic container containing water to keep the bone material in a moist environment. The bone pieces were not immersed in the water, however.

Individual fixtures containing the grafts were removed from the plastic container and indexing wheel one at a time to be measured. First, the reamed holes were cleaned with water and compressed 1,1,1,2 tetrafluorethane dust remover in an effort to remove machined bone chips. The assembling and grooving fixtures were then bolted into an aluminum adapter which was then bolted to the CMM table for measurement as shown in Figure 4-5.

The CMM software coordinate system was then aligned to the fixture as shown in Figure 4-6. First, a plane was created from five points on the top face of the support arm. This plane was defined as the z-plane into which all two-dimensional features would be projected. Next, a line was created from two points taken from left to right along the front face of the support arm to define the x-direction. A four-point circle was then taken inside of hole 1 the center of which defined the x- and y-direction zero. Finally, a single point was taken on the top face of the front clamp. This point, which was at the same level as the top of the stack-up, defined the z-direction zero. This sequence was completed first in the CMM manual operation mode and then in DCC mode. The y-direction vector was constructed in the PC-DMIS software as the cross product of the z-direction and the x-direction

Once the coordinate system was aligned to the graft, hole 1 and hole 2 were measured. Four ten-point circles were taken at 0.5 mm intervals along the axis of each hole (Figure 4-7). The diameter of each hole was defined as the average diameter of the four circles. Additionally, the straightness of each hole was calculated. To do this, the best-fit line through the centers of the four circles in the hole was determined. The straightness of the hole was then defined as the farthest distance of any given center from the best-fit line (Figure 4-8).

Loose cortical plates

The holes of the cortical plates were assigned a name by the convention "PL X-Y-Z". Here, the prefix "PL" designated the part as a plate. The "X" numeral was filled by a 1 or a 2 to designate the plate as the top or bottom plate in the fixture, respectively. The "Y" numeral indicated the position of the graft in the indexing wheel (1-6) and the "Z" numeral referred to the donor number (1-10). The hole designations described in the cortical-cancellous stack-up section were carried over to the loose plates.

Once a plate was removed from the machining fixture, one corner was removed with a razor blade as shown in Figure 4-9. This was done to keep track of the plate orientation throughout the remaining measurement cycles. The plate was then cleaned with water and compressed 1,1,1,2 tetrafluorethane to remove any remaining bone chips and excess water. It should be noted that no cleaning was performed on the parts after lyophilization and subsequent hydration. Excess water was wiped from the re-hydrated parts using a lint free tissue.

The loose cortical plates were then clamped to the CMM table as shown in Figure 4-10. The CMM coordinate system was aligned to the part as shown in Figure 4-11. Note that the removed corner is hidden by the clamp. First, a plane was constructed from six

points taken on the top face of the plate. This plane defined the z-plane into which all two-dimensional features were projected. Next, two circles were constructed from four points each in hole 1 and hole 2. A line from hole 1 to hole 2 was then constructed which defined the negative y direction. The x- and y-direction zero coordinates were shifted to the center of hole 1. Finally, a six-point plane was measured on the CMM table around the plate which defined the z-direction zero value. The x-direction was calculated as the cross product of the y-direction and z-direction. These features were measured first in manual operation mode and then in DCC mode to improve accuracy.

As with the clamped stack-ups, four 10-point circles were measured at 0.5 mm intervals in each of the plate holes. The diameter of each hole and the hole straightness were then calculated as described for the cortical-cancellous stack-ups.

Cortical pins

Cortical pins were received in a heat-sealed plastic bag. Once this bag was opened, the pins were coated with isopropyl alcohol then allowed to dry for 30 minutes. Individual pins were measured while clamped in a 5C collet (Figure 4-12).

Only the portions of the pin which would be in contact with the cortical plates were measured. Pins were therefore inserted into the collet such that 6.2 mm of pin length was exposed (Figure 4-13). This allowed 1 mm clearance from the portion of the pin to be measured to the top of the collet.

As with the other part types, the first step in the measurement process was to align the CMM coordinate system to the pin (Figure 4-14). First, a plane was constructed from five points on the top flat surface of the manual collet holder to which the z-plane was leveled. Next, a four-point circle was measured around the pin, the center of which defined the x- and y-coordinate zero values. Finally, a single point was taken on the top

surface of the pin which defined the z-coordinate zero. Due to the nominally axisymmetric shape of the pin, the x- and y-directions were not explicitly defined. As with other part types, this alignment was performed first in manual operation mode then in DCC mode.

The non-chamfered end of the pin was measured first using eight 10-point circles at 0.5 mm intervals along the length of the pin shaft (Figure 4-15). The pin was then removed from the collet, re-clamped with the chamfered end exposed, and measured in the same fashion. Finally, the non-chamfered end was re-measured. The first measurement of the non-chamfered end was not used in determining the dimensions of the pin.

The pin diameter was calculated as the average of the 16 diameter values taken from both ends of the pin (Figure 4-16). The straightness error of either end was determined by constructing a best-fit line through the centers of the eight circles, then calculating the maximum center deviation from that line. The pin straightness error was defined as the larger straightness error from the two ends.

Unlike the cortical plates, which were designated according to their location in the machining fixture, cortical pins could not be given a designation until after they were measured and paired to an allograft, whether or not that graft would later be assembled. Pins were named according to the convention “PN X-Y-Z”. Here, the “X” numeral designated whether the pin was to be inserted into hole 1 or hole 2 of its corresponding graft. The “Y” numeral designated the station of the indexing wheel containing the stack-up into which the pin would be inserted. Again, this designation carried over even if that

graft was in stations 4-6 and would not be assembled. Finally, the "Z" place holder indicated which donor the pin came from.

Pull-apart Tests

The quality of the interference fit of the assembled allografts was experimentally investigated by measuring the force required to separate a cortical plate from its two interference pins. These tests were carried out using an MTS Q-Test 5 Load Frame with Testworks 4 software. The load frame was fitted with a 5 kN load cell and mechanical grips as in Figure 4-17.

The grafts to be tested were fixed with epoxy to grooved aluminum blocks which were clamped in the mechanical grips. This was done to avoid the need to clamp the cortical plates and thereby affect the interference connection. The 3.2 mm (1/8 in.) grooves in the aluminum blocks prevented the pins from being glued to the aluminum or the cortical plates.

Prior to any mechanical testing, the grafts were tested by hand as done in the RTI production environment. To do this, each cortical plate was held between the thumb and index finger of one hand and tension was applied. If any resistance was met, tension was ceased. Grafts that separated with no appreciable resistance were reassembled and retested as described in the following sections.

Sample preparation

The aluminum blocks were first filed to remove any residual epoxy from previous tests, then roughened with 60 grit sand paper to improve the ability of the epoxy to bond. The blocks were sonicated in acetone and methanol, rinsed with water, and blown dry with compressed air.

The grafts were then epoxied to the aluminum blocks. A quick-setting epoxy was used for donors 1-6. X of the Y tests for these donors resulted in the failure of the epoxy bond rather than the interference fit. For that reason, a metal and concrete epoxy was used for donors 7-10. After a five minute curing period, the bond was reinforced by applying more epoxy to the sides of the cortical plates. The epoxy was then allowed to cure for 24 hours. Just prior to tensile testing, the grafts were immersed in water for 30 seconds as per RTI specifications.

Pull-apart test procedure

The allograft and aluminum block assembly was fixed in the load frame grips. A ground parallel block was used to help align the assembly to the tensile direction of the load frame. The lower grip was tightened on the lower aluminum block first. While the upper grip was being tightened, the position of the load frame crosshead was adjusted to keep the load on the graft as close to zero as possible.

When the allograft-aluminum assembly was fixed in the grips, the tensile load was increased at a nominal rate of 20 N/s until the crosshead had moved by 3.5 mm, indicating that the graft had separated or broken free from an aluminum block. During the tests, load, crosshead position, and time were recorded by the MTS software. The peak force in the load cycle was taken to be the pull-apart force.

Finite Element Analysis

A finite element model of the interference fit was created to both predict allograft failures and validate/improve the isotropic model used in the Monte Carlo simulation.

ANSYS 10 software was used to create the solid model and mesh as well as to complete the analysis (Figure 4-18). To simplify the model, the 11 mm radius on the top of the graft was neglected. The diameter of the pin in this model was given a value equal

to the average of all pin diameters from the dimensional study. The diameter of the holes was made equal to the pin diameter minus the average predicted interference value from the dimensional study. Twenty-node brick elements were used to populate the pin and the plate. To simulate the interference fit, contact and target elements were created at the pin-plate interfaces.

A two-step load scenario was used to study the interference fit. First, a static study was used to model the stresses in the assembled allograft. Von Mises equivalent stress values and contact pressures observed after this load step. Next, a relative motion of 100 μm was applied to one end of both pins to induce slippage. The pull-apart force was then found by summing the z-direction forces of all of the contact elements.

Analytical Model and Monte Carlo Simulation

An analytical interference fit model formed the basis for a Monte Carlo simulation used to predict the rate of pull-apart failure of the assembled grafts. The analytical model applied in this simulation was discussed in Chapter 2. This model assumes isotropic material properties and a cylindrical geometry of both pin and plate.

The purpose of the Monte Carlo simulation was to serve as a tool for predicting the frequency of interference fit failures, either by insufficient pull-apart force or yielding. Additionally, the simulation was used to compare the relative influence of the different model parameters. The Monte Carlo simulation was written in Matlab (see Appendix).

To estimate the frequency of failure, each input parameter in Table 4-1 was assigned a mean value and standard deviation. Mean values and standard deviations of geometric variables were taken from the results of the dimensional study. Values for the elastic constants were obtained from the literature (Chapter 2). The stress concentration

factor Kt and the effective plate outer radius were obtained by comparison with the finite element model (see Chapter 5).

The Monte Carlo simulation was then used to generate histograms which predicted the number of occurrences of both negative pull-apart forces and Von Mises stress values above the failure stress. This was done by selecting values for each of the variables in Table 4-1 randomly within one standard deviation of their mean value. Forces and stresses were then calculated according to the analytical model discussed in Chapter 2. Von Mises stress was only calculated when the interference was greater than zero. This process was repeated 250,000 times to generate a distribution of outputs.

The relative influence of individual variables could then be tested by setting the standard deviation values for all variables, except the variable of interest, to zero. The resultant standard deviation of the pull-apart force distribution could then be compared to similar simulations for other variables to determine the most influence factors on the interference fit.

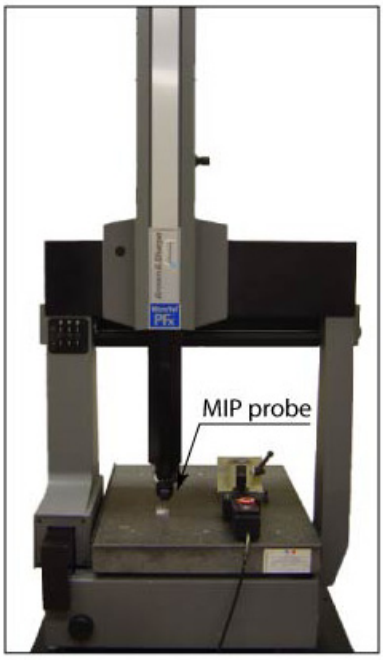

Figure 4-1. Brown and Sharpe MicroVal PFx coordinate measuring machine.

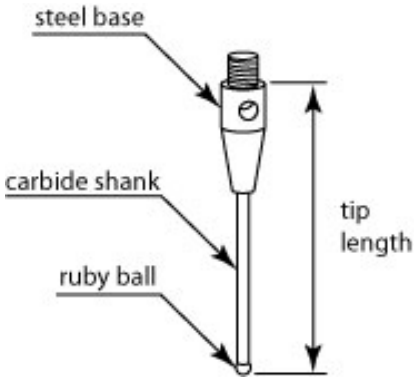

Figure 4-2. Probe tip geometry used in this study.

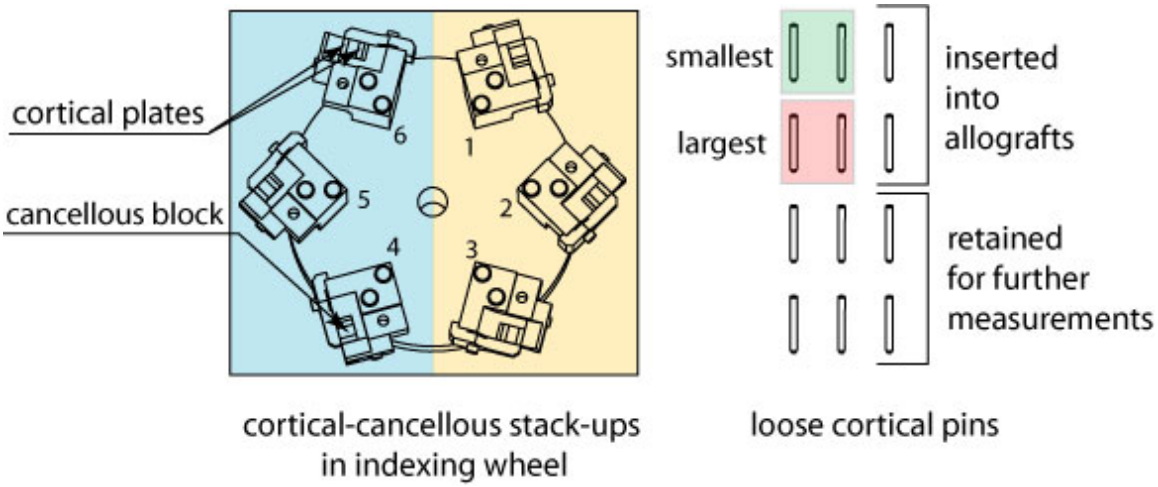

Figure 4-3. Allograft parts as received from RTI for one donor. Cortical-cancellous stack-ups 1-3 as marked above were assembled into allografts. Stack-ups 4-6 were removed from the assembling and grooving fixture for further measurement.

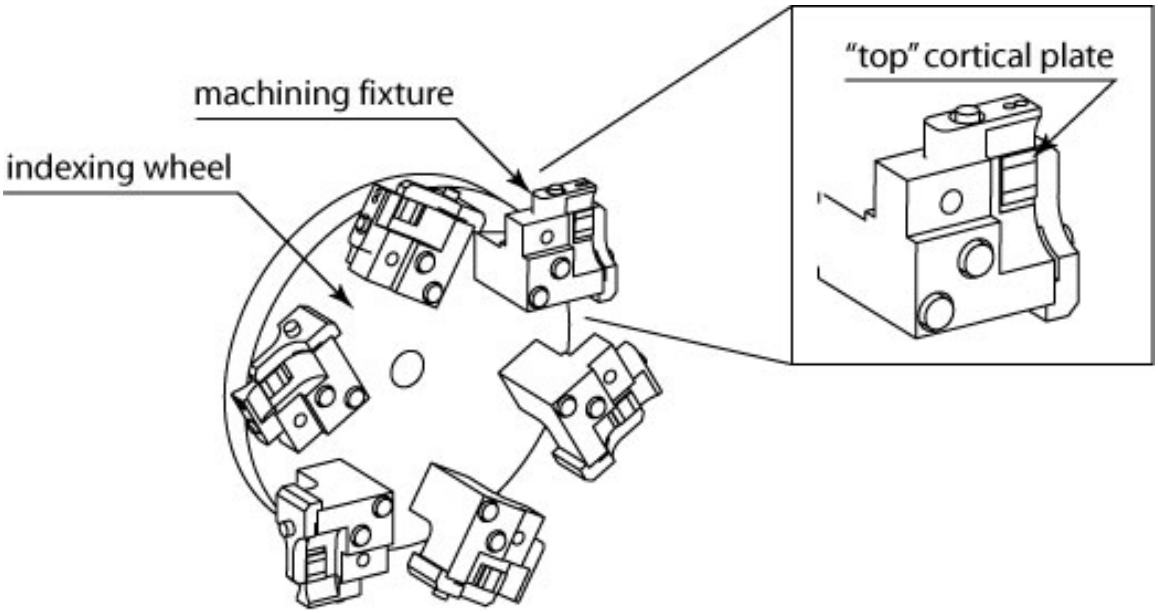

Figure 4-4. RTI indexing wheel and assembling/grooving fixtures. Only the top cortical plate could be measured in this fixture due to probe tip length limitations.

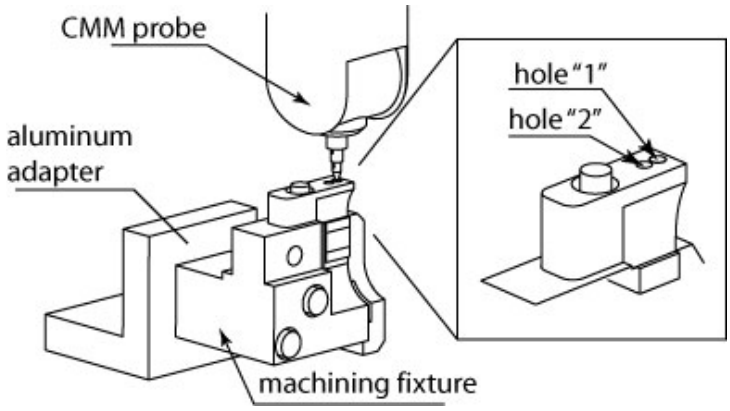

Figure 4-5. Stack-up measurement. Inset shows hole naming convention.

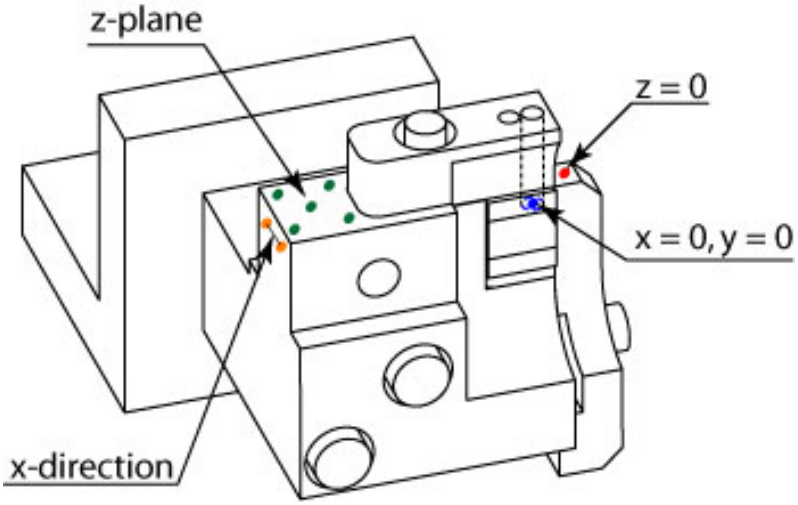

Figure 4-6. Stack-up coordinate system alignment features.

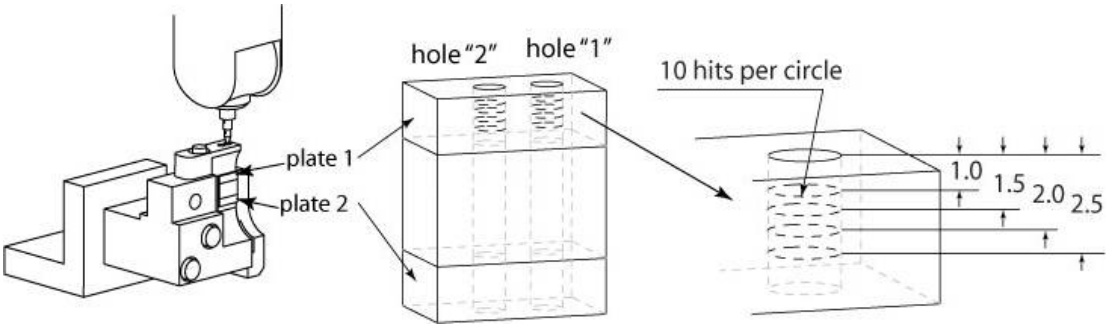

Figure 4-7. Measurement of the cortical plates while stacked in the machining fixture.

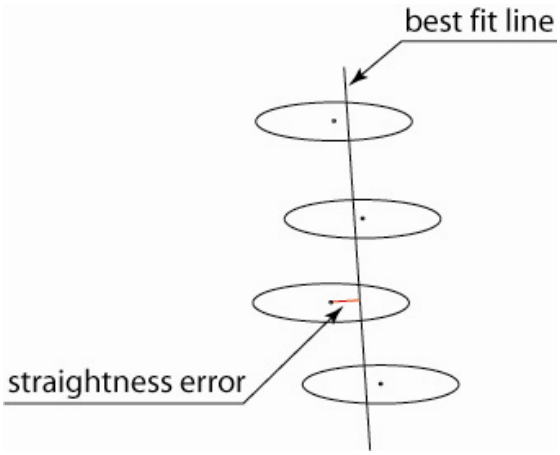

Figure 4-8. Definition of straightness error.

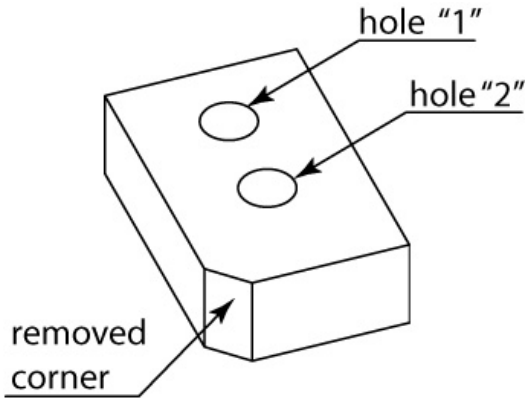

Figure 4-9. One corner of each loose plate was removed to preserve orientation.

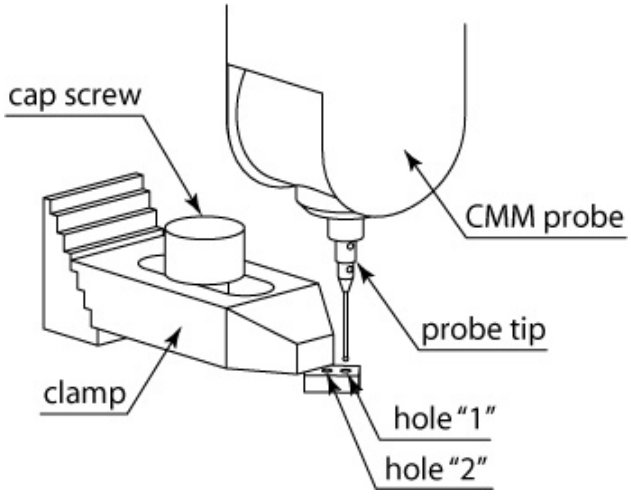

Figure 4-10. Loose cortical plates were clamped directly to the CMM table.

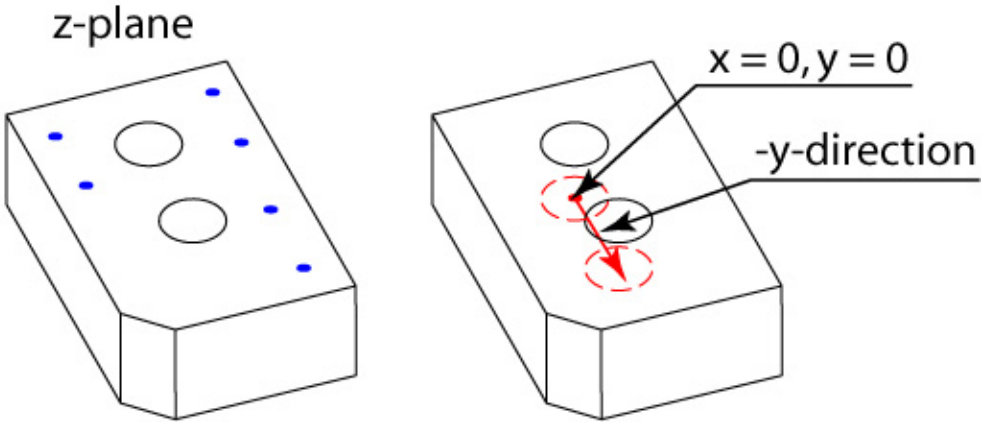

Figure 4-11. Cortical plate coordinate system alignment features.

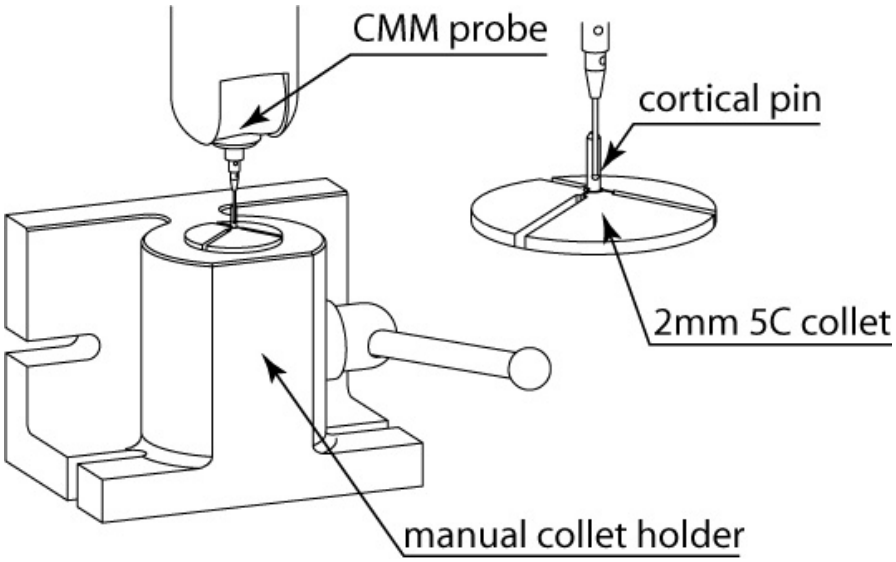

Figure 4-12. Cortical pins were measured while clamped in a 5-C collet and manual collet holder.

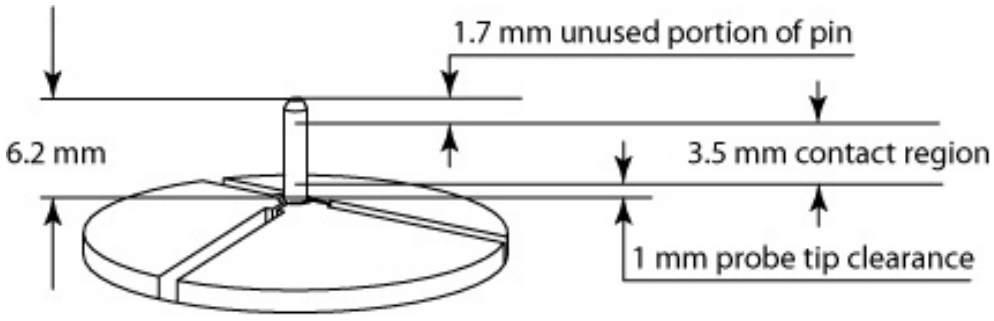

Figure 4-13. Pins were clamped in the collet with 6.2 mm of length exposed.

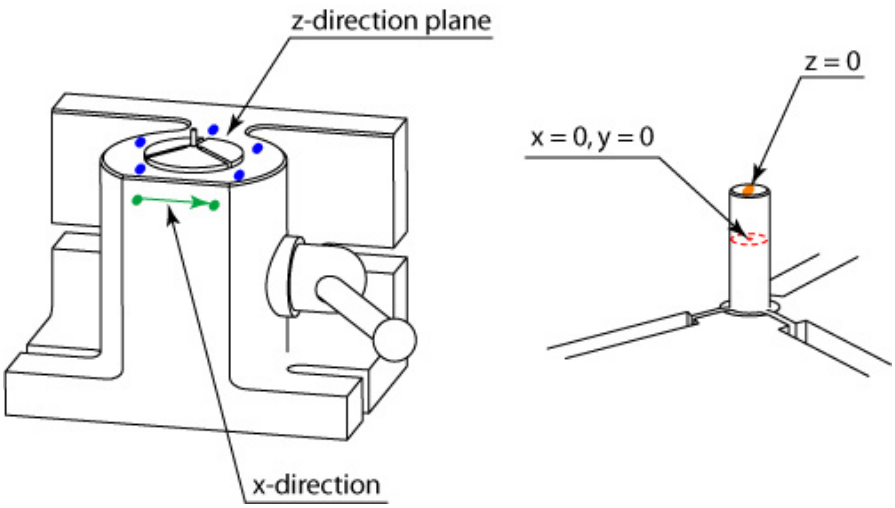

Figure 4-14. Cortical pin coordinate system alignment features.

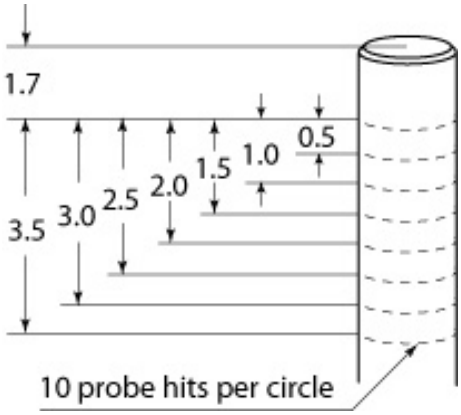

Figure 4-15. Measurement locations for one side of the cortical pin.

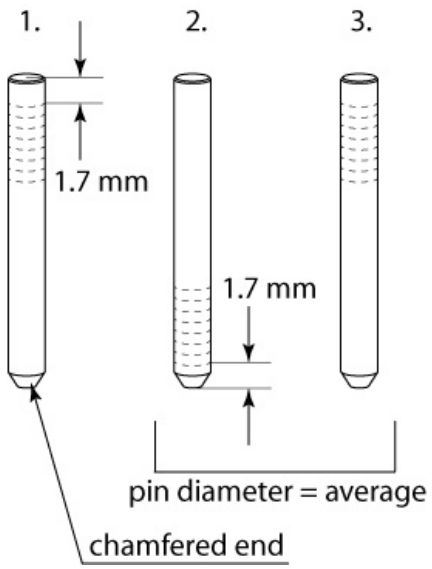

Figure 4-16. Cortical pin measurement procedure. 1. Measure non-chamfered end. 2. Measure chamfered end. 3. Measure non-chamfered end again to investigate effects of collet clamping.

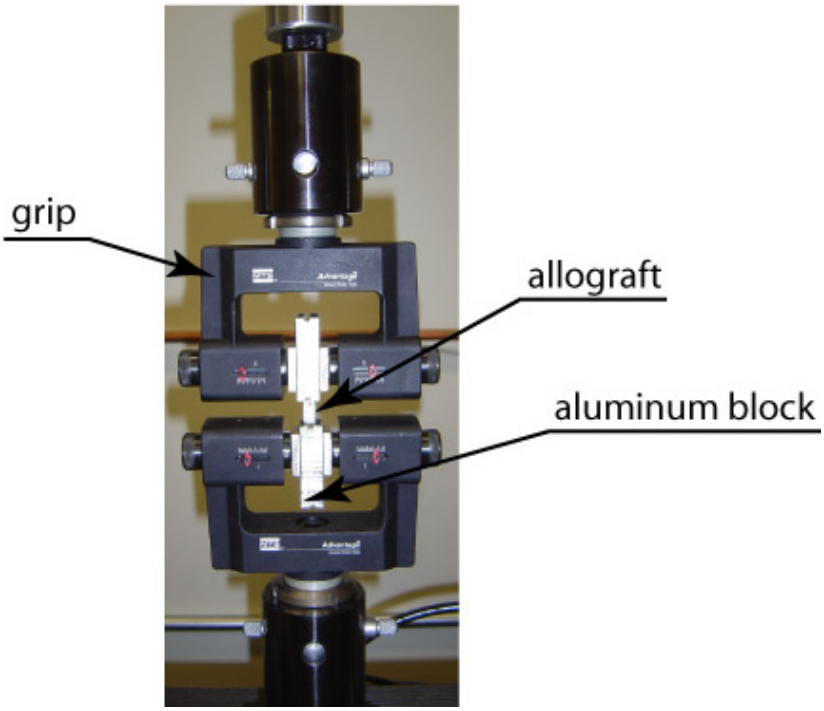

Figure 4-17. Pull-apart test setup.

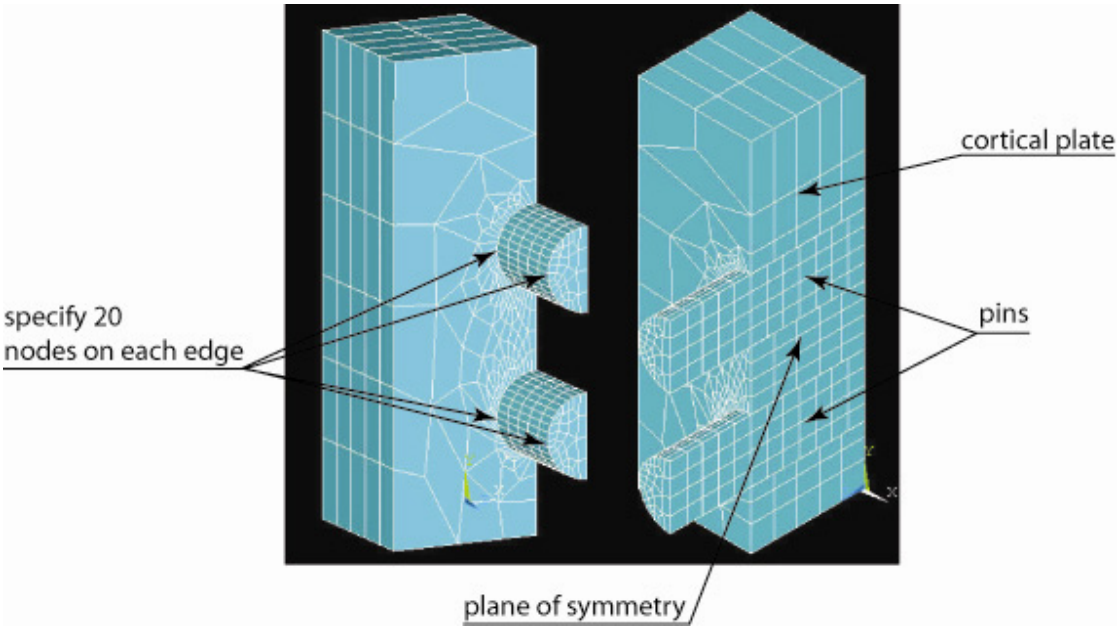

Figure 4-18. The ANSYS model and mesh used in the finite element analysis.

Table 4-1. Input parameters for the Monte Carlo analysis

Parameter	Symbol
Radial Interference	δ
Young's Modulus (Pin)	Ei
Young's Modulus (Plate)	Eo
Poisson's Ratio (Pin)	μi
Poisson's Ratio (Plate)	μo
Interface Radius	b
Effective Plate Radius	c
Stress Concentration	Kt
Length of Contact	L
Friction Coefficient	μf

CHAPTER 5
RESULTS AND DISCUSSION

The following sections contain the results of the dimensional measurements, pull-apart tests, finite element analyses, and Monte Carlo simulation. Additionally, results are presented for the friction testing that was performed in support of the finite element and Monte Carlo models.

Dimensional Measurements

As was discussed in previous chapters, dimensional measurements were completed both to understand the accuracy and consistency of the RTI manufacturing process as well as to use in predictive models of the interference fit. To this end, results are presented first for the pins and plate holes separately, then for the combined interference of the allograft components.

Interference Pins

Average diameter values by donor are shown in Table 5-1. Note that the diameters from the first, second, and third donors have substantially larger diameters than those pins from the other seven donors. A tool change was performed on the lathe used to turn the pins between the times when donors 3 and 4 were processed. Also note that while the diameter values stay relatively constant after BioCleanse™, lyophilization causes the pin diameters to drop by an average of 50 μm. Subsequent hydration of the pins for 30 s results in an average diametric recovery of 11 μm.

Also included in Table 5-1 are the average diameter values measured with calipers by the RTI machinist for each donor. Since these diameter values represent the ‘bin’ to

which the pins were assigned, and thereby determine the reamer sized used in drilling the plate holes, their accuracy is of some importance. The RTI-measured average diameter values deviate by anywhere from 1 μm to 12 μm from the diameters measured as-machined using the Brown and Sharpe CMM. Recall from Chapter 3 that reamer sizes are available in 0.0005 in (12.7 μm) increments.

Measurement repeatability

Before further comments can be made on the measurement results for the pin diameters, it is first necessary to quantify the reliability of the CMM measurements. To that end, the results of ten repeated measurements of a single pin are shown in Table 5-2. Between each repetition, the pin is removed and re-fixtured in the collet. Over the ten measurements, the measured pin diameter varies over a 6 μm range with a standard deviation of 2 μm.

Taper characterization

RTI manufacturing drawings call out a maximum taper of 0.0005 in (12.7 μm) over the length of a pin. In this study, the taper of the pins is investigated in three ways. First, the range of diameter values over the sixteen circles measured on each pin is recorded (Figure 5-1). Average single-pin diameter range values are tabulated by donor and manufacturing process in Table 5-3. It should be noted average values for donor 3 are consistently out of specification. However, after lyophilization and re-hydration, only one of the pins from donor three was actually out of specification at 15 μm of variation. The average value for donor 3 was skewed due to the fact that two pins were lost during the BioCleanse™ cycle. Also note that the average single-pin diameter range for each process stays relatively constant, but is slightly higher after lyophilization. Eight of fifty-

seven loose pins that completed the manufacturing process had a "taper" of greater than 12.7 μm.

Next, pin straightness error, as defined in Chapter 4, is calculated as the deviation of circle center locations from a best fit line through all measured circles (Figure 4-8). Average pin straightness error values for each donor and manufacturing process are recorded in Table 5-4. Note that the average straightness error stays consistent to within 4 μm for each donor.

Finally, a comparison between the diameters of the chamfered and non-chamfered ends of each pin (Figure 5-2) is made in order to ensure that one end of the pin is not systematically larger than the other. The average diametric difference between the two ends of each pin are recorded for each donor and manufacturing cycle in Table 5-5. Here, the diametric difference is defined as the average diameter of the non-chamfered end minus the average diameter of the chamfered end.

Table 5-5 indicates that while one end may be larger than another for a given pin or even for the pins from a given donor, this difference is small compared to the repeatability of pin measurements shown in Table 5-2. More significant from a manufacturing standpoint, neither end is consistently larger or smaller than the other as one might expect from turning a cantilevered beam (see Chapter 3).

Collet clamping effects

One item of concern when fixing the pins for measurement on the CMM was that the collet was plastically compressing the bone material. To investigate the possibility of permanent deformation, the non-chamfered end of each pin was measured twice. The average difference of the second diameter measurement minus the first, the "clamping

effect", is catalogued for each donor in Table 5-6. The collet clamping effect, while generally 0-2 μm, is most notable prior to lyophilization for larger diameter pins.

Pin manufacturing repeatability

For each donor, the range of diameters for the six pins not inserted into allografts was calculated as shown in Figure 5-3. This was done to gain some understanding of the repeatability of each stage in the manufacturing process. The pin diameter variation for each donor at each manufacturing cycle is shown in Table 5-7. It should be noted that the average single-donor diameter variation decreases after BioCleanse™ and increases dramatically after lyophilization.

Cortical Plate Holes

Average cortical plate hole diameters for each donor and manufacturing step are shown in Table 5-8 along with the corresponding reamer diameter used by RTI. Like the pin diameters, the plate hole diameters fall dramatically, here by an average of 29 μm, after lyophilization. However, unlike the cortical pins, 30 seconds of immersion in water only recovers an average of 3 μm of diameter.

Hole diameter measurement repeatability

As with the cortical pins, ten repeat measurements were taken of a single cortical plate hole. The results of these repeat measurements are shown in Table 5-9. Over the 10 measurements, a standard deviation of 0.005 mm from the mean value is observed.

Effects of the RTI machining fixture

As was discussed in Chapter 4, the cortical plates are measured both in the RTI machining fixture and clamped to the CMM table to determine whether any diametric change occurs. Table 5-10 shows the average discrepancy between the two sets of measurements. The loose plates are on average 6 μm larger than the plates measured in

the machining fixture with a standard deviation of 7 μm. This relatively large variance in the effect of the fixture may be due to variations in the cortical plate exterior dimensions. Since the front and side clamps of the machining fixture are tightened to be flush with the fixture body, rather than to a set force, the amount of stress and strain that a plate is subjected to could vary significantly if the plate was oversized or undersized.

Accompanying Table 5-10 are the results of a ten repeated measurements of a cortical plate hole clamped in a machining fixture (Table 5-11). Note that the range and standard deviation of the values are comparable to those in Table 5-9.

Straightness error

Table 5-12 shows the average straightness error values of the cortical plate holes sorted by donor and manufacturing cycle. Average straightness error values for the cortical pin holes range from 2 μm to 10 μm and do not vary more than 4 μm over the various stages of the manufacturing process. These results are similar to those seen for the cortical pins.

Diametric variation between the two plate holes

Table 5-13 shows the average diametric variation between the two holes of a given cortical plate. Here, the diametric variation is defined as the diameter of hole "2" minus the diameter of hole "1". Table 5-13 indicates that, on average, hole "1" is 2-3 μm larger than hole "2", though with a standard deviation of 3-5 μm, regardless of the manufacturing cycle.

Diametric variation between plates

Table 5-14 shows the average diametric variation between the holes of the two cortical plates of a given allograft. Here, diametric variation is defined as the average diameter from plate "2" minus the average diameter from plate "1". Table 5-14 indicates

that once the plates complete the manufacturing process, little difference exists between the diameters of the two plates.

Manufacturing process repeatability

As with the cortical pins, it is desirable not just to know the accuracy of the hole diameter values, but also their precision. The quality and repeatability of the drilled and reamed holes are characterized in two ways. First, the single-plate range of diameter values is calculated as shown in Figure 5-4. Table 5-15 shows the average values of the single-plate diameter range for each donor and manufacturing cycle. On average, the diameters of the holes of a given plate vary by 10-11 μm.

Additionally, the range of hole diameters over a single donor is calculated as shown in Figure 5-5. The results of these calculations are shown in Table 5-16, which indicates significant diametric variation from hole to hole. At the end of the manufacturing process, the twelve cortical plate holes associated with a given donor will vary by an average of 17 μm.

Diametric Interference

Table 5-17 shows the average predicted diametric interference between the cortical pins and the cortical plate holes for each donor and each manufacturing process. Here, the predicted diametric interference is defined as the calculated diametric difference between the pins and plate holes that were not formed into allografts. Recall from Chapter 3 that RTI specifies a machined diametric interference of 0.0010-0.0015 in. (25-38 μm). Table 5-17 indicates that with the exception of donor 9, the average interference values after machining are within acceptable limits. The predicted interference drops by an average of 21 μm after lyophilization and recovers by an average of 7 μm after thirty seconds of immersion in water. Donor 9 is of particular note since the predicted interference values

become negative after lyophilization. Also note that the standard deviation of the interference values are a much larger percentage of the average values after lyophilization and rehydration than after machining and BioCleanse™.

Mechanical Pull-apart Tests

Table 5-18 shows the results for the mechanical pull-apart tests including occurrences of manual pull-apart failures, the plate that failed, which epoxy was used and the load at which failure occured. As discussed in Chapter 4, the allografts were first tested manually for pull-apart failure after lyophilization and before hydration. Out of the thirty grafts considered in this study, 4 (13%) failed during manual testing and 17 (57%) exhibited visible cracking in one or both cortical plates. None of the grafts that failed the manual pull-apart test were made from sets of pins and plates deliberately matched to have poor interference. All of the cracks were in the longitudinal bone direction and ran from the pin to the edge of the plate.

Of the 30 assembled allografts, 20 were pulled apart during mechanical testing. For the remaining 10 grafts, the epoxy holding the graft to the aluminum blocks failed before the interference fit. Results for the 20 grafts that were pulled apart are listed in Table 5-19. The average pull-apart force was found to be 83.4 N with a standard deviation of 25.9 N. The average pull-apart force of the grafts with no cracks was found to be 100.6 N with a standard deviation of 28.5 N. The average pull-apart force of the grafts what exhibited cracks was found to be 74.1 N with a standard deviation of 19.8 N.

Also included in Table 5-19 are the predicted interference values for each graft after machining and adjusted by the average process effect for each donor after lyophilization and hydration. Here, the predicted interference after machining is

calculated as the difference between the average pin diameter and average hole diameter for each graft.

Figure 5-6 shows the pull-apart force plotted against donor number and the predicted interference values. Unexpectedly, Figure 5-6 indicates little or no correlation between the predicted diametric interference and the pull-apart force. This could indicate that over the small sample size (the seven grafts that were pulled apart that did not exhibit cracking) variations in material properties play a larger role than dimensional interference. It is also possible that the poor correspondence between predicted interference and pull-apart force reflects a difference in the effects of lyophilization and hydration on the assembled graft as opposed to the measured loose parts.

Finite Element Analysis

The finite element analysis described in Chapter 4 was completed three times with three separate sets of material property and geometric inputs (Table 5-20). Here, the subscript "r" refers to the radial bone direction, the subscript "c" refers to the circumferential bone direction, and the subscript "l" refers to the longitudinal bone direction. The von Mises stress and pull-apart force results from each trial are shown in Table 5-21. For the first trial, the material properties were taken from [16] while the pin diameter and diametric interference were taken from the measurement results after hydration. The second trial used the same material properties as the first trial but used geometric values associated with the lyophilized state. The third trial used a pin diameter and interference equal to those of the second trial, but used mechanical properties reduced by roughly one standard deviation from the values used in the first two trials. Of the three trials, the third trial (reduced modulus and interference values) shows the closest agreement to the experimental data.

The von Mises stress distribution and contact pressure plot for the third trial are shown in Figures 5-7 and 5-8, respectively. Not surprisingly, the highest stresses are located at the contact and between the two pins. Somewhat more surprising is the absence of a defined stress concentration at the edge of the edge of the contact where the pins overlap the holes.

Monte Carlo Simulation

The Monte Carlo simulation inputs are shown in Table 5-22. Interference values and pin diameter values are taken from the measured results after lyophilization. Mean Young's modulus values are the same as the radial and circumferential values from the finite element model. The Young's modulus standard deviation, as well as the Poisson's ratio mean and standard deviation values, are selected from.[16] According to the finite element analysis results, a stress concentration factor of 1 was used. Finally, the effective plate outer radius was adjusted until the simulation results best matched the finite element results.

The output statistical distributions from the multi-parameter Monte Carlo simulation are shown in Table 5-23 and Figure 5-9. Note that the mean pull-apart force is within the range of results observed in the mechanical testing while the pull-apart force standard deviation is dramatically higher. This suggests that the Monte Carlo analysis is overstating the variation in the actual force and stress levels.

The model indicates a pull-apart failure ($F < 0$) rate of 13%. Recall from the mechanical testing that the pull-apart failure rate was also found to be 13%. Assuming a failure stress of 25 MPa (the ultimate tensile strength reported by Bianchi [5]), the simulation predicts a von Mises stress failure rate in the cortical plates of 84%. If the tensile failure stress is assumed to be 53 MPa (as reported by Reilly and Burstein [16]), the

simulation predicts that 57% of the grafts will fail. Recall from the mechanical testing that the 57% of the allografts were found to have cracks in them.

Table 5-24 shows the results of the single-parameter variation simulation. The simulation indicates that the diametric interference, coefficient of friction, and plate Young's modulus are the most influential parameters on the pull-apart force. Also, the simulation indicates that diametric interference, plate Young's modulus, and bone Poisson's ratio are the most influential factors on the von Mises stress in the cortical plate. Note that the prediction that diametric interference is the most influential factor in the quality of the interference fit is not supported by the pull-apart data.

Table 5-1. Average pin diameters in mm by donor over the RTI manufacturing step.

Donor	RTI Measured	Machined	BioCleanse™	Lyophilization	Rehydrated
1	2.014	2.013	2.014	1.958	1.975
2	2.014	2.021	2.024	1.965	1.994
3	2.010	2.012	2.014	1.965	1.965
4	1.976	1.970	1.975	1.930	1.937
5	1.980	1.975	1.977	1.930	1.939
6	1.980	1.968	1.973	1.926	1.931
7	1.978	1.967	1.973	1.937	1.945
8	1.975	1.970	1.976	1.934	1.945
9	1.975	1.962	1.970	1.903	1.918
10	1.970	1.968	1.974	1.921	1.926
Max	2.014	2.021	2.024	1.965	1.994
Min	1.970	1.962	1.970	1.903	1.918
Range	0.044	0.059	0.054	0.061	0.076
St. Dev.	0.018	0.023	0.021	0.020	0.024
Average	1.987	1.983	1.987	1.937	1.948

Table 5-2. Pin measurement repeatability.

Trial	Pin Diameter (mm)
1	1.955
2	1.954
3	1.955
4	1.953
5	1.953
6	1.953
7	1.953
8	1.952
9	1.951
10	1.957
Max	1.957
Min	1.951
Range	0.006
St. Dev	0.002
Average	1.954

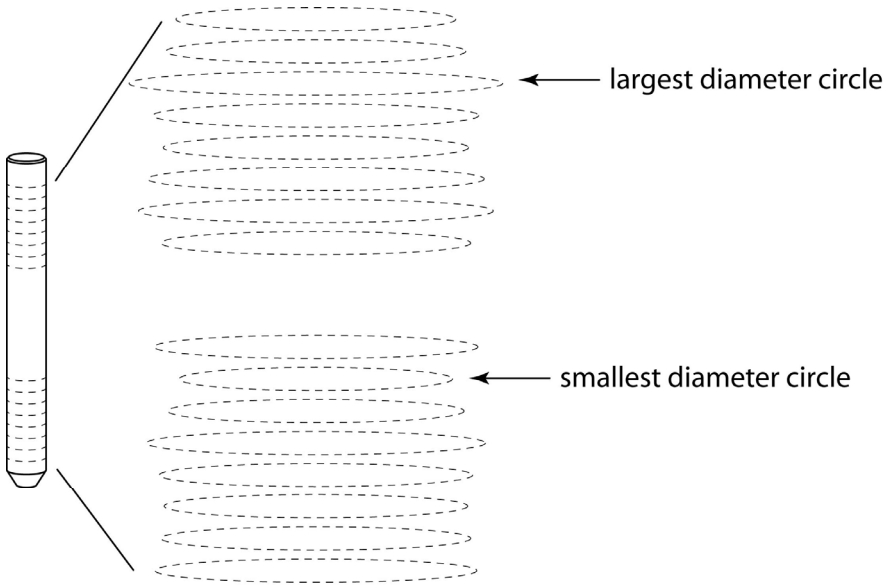

Figure 5-1. Diameter range over a single pin. Diameter variation graphically exaggerated for clarity.

Table 5-3. Average single-pin diameter range values in mm by donor and manufacturing process.

Donor	Machined	BioCleanse™	Lyophilization	Rehydrated
1	0.010	0.014	0.017	0.013
2	0.009	0.010	0.010	0.010
3	0.014	0.016	0.016	0.010
4	0.010	0.012	0.015	0.013
5	0.006	0.006	0.006	0.006
6	0.005	0.006	0.004	0.006
7	0.008	0.006	0.007	0.006
8	0.007	0.007	0.007	0.007
9	0.011	0.008	0.009	0.009
10	0.012	0.008	0.006	0.005
Max	0.014	0.016	0.017	0.013
Min	0.005	0.006	0.004	0.005
St. Dev.	0.003	0.004	0.005	0.003
Average	0.009	0.009	0.010	0.009

Table 5-4. Average pin straightness error values in mm.

Donor	Machined	BioCleanse™	Lyophilization	Rehydrated
1	0.007	0.011	0.008	0.008
2	0.005	0.006	0.006	0.005
3	0.005	0.008	0.006	0.007
4	0.006	0.008	0.009	0.010
5	0.003	0.003	0.003	0.005
6	0.004	0.004	0.003	0.004
7	0.003	0.004	0.004	0.003
8	0.005	0.005	0.005	0.005
9	0.004	0.003	0.005	0.005
10	0.003	0.004	0.004	0.003
Max	0.007	0.011	0.009	0.010
Min	0.003	0.003	0.003	0.003
St. Dev.	0.001	0.003	0.002	0.002
Average	0.004	0.006	0.005	0.006

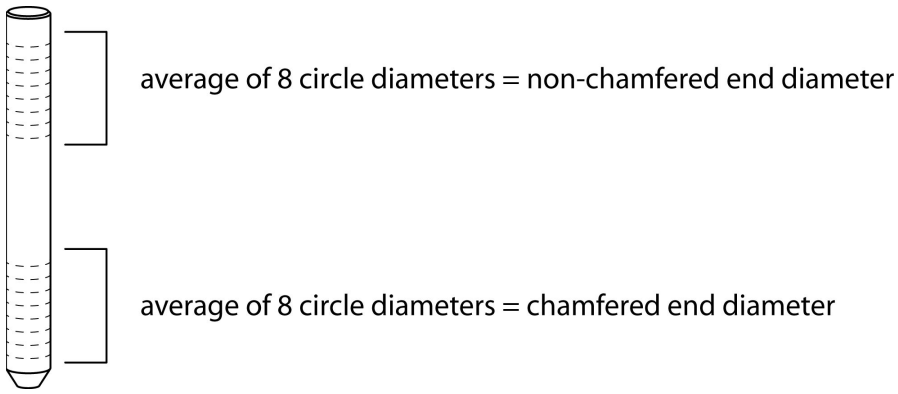

Figure 5-2. Comparison of average diameters of the two pin ends.

Table 5-5. Diametric differences in mm between the chamfered and non-chamfered pin ends.

Donor	Machined	BioCleanse™	Lyophilization	Rehydrated
1	0.003	0.005	0.007	0.004
2	-0.002	-0.002	-0.001	0.000
3	0.002	0.003	0.005	0.001
4	0.000	0.001	0.003	0.001
5	0.000	-0.001	0.001	0.000
6	0.000	-0.001	-0.001	-0.002
7	0.000	0.000	0.000	-0.001
8	0.000	-0.002	0.001	-0.002
9	0.001	0.000	0.000	-0.001
10	0.001	-0.001	0.001	-0.001
Max	0.003	0.005	0.007	0.004
Min	-0.002	-0.002	-0.001	-0.002
St. Dev.	0.001	0.002	0.003	0.002
Average	0.000	0.000	0.001	0.000

Table 5-6. Average collet clamping effect in mm.

Donor	Machined	BioCleanse™	Lyophilization	Rehydrated
1	-0.005	-0.005	0.000	-0.002
2	-0.004	-0.003	0.000	-0.001
3	-0.003	0.002	0.002	-0.001
4	-0.001	-0.002	0.000	0.001
5	-0.002	-0.002	0.001	0.000
6	-0.001	-0.001	0.000	0.000
7	-0.001	-0.001	0.000	0.000
8	0.000	-0.001	0.000	-0.002
9	-0.002	-0.001	0.000	0.001
10	-0.001	-0.001	0.001	0.000
Max	0.000	0.002	0.002	0.001
Min	-0.005	-0.005	0.000	-0.002
Range	0.004	0.006	0.002	0.003
St. Dev.	0.001	0.002	0.001	0.001
Average	-0.002	-0.001	0.000	0.000

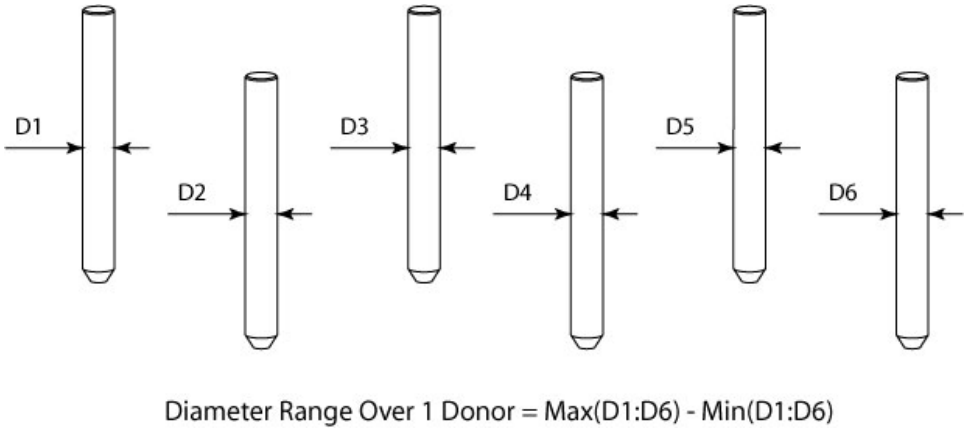

Figure 5-3. Pin diameter variation over a single donor

Table 5-7. Variation of pin diameters in mm across a single donor.

Donor	Machined	BioCleanse™	Lyophilization	Rehydrated
1	0.008	0.010	0.024	0.028
2	0.014	0.008	0.019	0.012
3	0.008	0.008	0.018	0.022
4	0.011	0.007	0.018	0.019
5	0.012	0.004	0.008	0.011
6	0.008	0.003	0.010	0.008
7	0.015	0.007	0.017	0.017
8	0.016	0.007	0.017	0.015
9	0.022	0.011	0.036	0.027
10	0.008	0.009	0.015	0.014
Max	0.022	0.011	0.036	0.028
Min	0.008	0.003	0.008	0.008
Range	0.014	0.008	0.028	0.020
St. Dev.	0.005	0.002	0.008	0.007
Average	0.012	0.007	0.018	0.017

Table 5-8. Average cortical plate hole diameters (mm) by donor and manufacturing process.

Donor	RTI Reamer	Machined	BioCleanse™	Lyophilization	Rehydrated
1	1.981	1.968	1.983	1.952	1.951
2	1.976	1.978	1.982	1.953	1.961
3	1.976	1.984	1.982	1.962	1.961
4	1.943	1.937	1.947	1.918	1.915
5	1.943	1.927	1.946	1.913	1.918
6	1.938	1.938	1.939	1.907	1.913
7	1.943	1.932	1.938	1.909	1.915
8	1.941	1.941	1.949	1.923	1.922
9	1.938	1.944	1.944	1.910	1.914
10	1.930	1.930	1.941	1.910	1.925
Max	1.981	1.984	1.983	1.962	1.961
Min	1.930	1.927	1.938	1.907	1.913
Range	0.051	0.057	0.045	0.055	0.048
St. Dev.	0.019	0.021	0.019	0.021	0.020
Average	1.951	1.948	1.955	1.926	1.929

Table 5-9. Ten repeated measurements of one cortical plate hole.

Trial	Hole Diameter (mm)
1	1.915
2	1.921
3	1.923
4	1.926
5	1.927
6	1.928
7	1.929
8	1.930
9	1.931
10	1.931
Max	1.931
Min	1.915
Range	0.016
St. Dev.	0.005
Average	1.926

Table 5-10. Effects of the RTI machining fixture on hole diameter.

	Average "Plate 1" Hole Diameter		
Donor #	In Mach. Fixt. (mm)	Loose Plates (mm)	Discrepancy (mm)
1	1.964	1.978	0.014
2	1.971	1.978	0.006
3	1.969	1.982	0.013
4	1.934	1.932	-0.002
5	1.932	1.933	0.002
6	1.929	1.937	0.008
7	1.933	1.925	-0.008
8	1.933	1.943	0.010
9	1.937	1.944	0.007
10	1.926	1.936	0.010
Max			0.014
Min			-0.008
Range			0.022
Std Dev			0.007
Mean			0.006

Table 5-11. Ten repeated measurements of a cortical plate hole diameter (mm) while clamped in the RTI machining fixture.

Trial	Hole Diameter
1	1.924
2	1.925
3	1.928
4	1.934
5	1.936
6	1.933
7	1.936
8	1.935
9	1.933
10	1.934
Max	1.936
Min	1.924
Range	0.012
St. Dev.	0.004
Average	1.932

Table 5-12. Average straightness error (mm) of cortical plate holes by donor and manufacturing cycle.

Donor	Machined	BioCleanse™	Lyophilization	Rehydrated
1	0.003	0.003	0.003	0.007
2	0.004	0.002	0.002	0.002
3	0.005	0.006	0.006	0.008
4	0.006	0.006	0.006	0.007
5	0.009	0.010	0.006	0.006
6	0.002	0.006	0.008	0.003
7	0.003	0.005	0.004	0.006
8	0.004	0.004	0.003	0.004
9	0.002	0.002	0.003	0.002
10	0.005	0.003	0.005	0.003
Max	0.009	0.010	0.008	0.008
Min	0.002	0.002	0.002	0.002
Range	0.007	0.008	0.006	0.005
St. Dev.	0.002	0.003	0.002	0.002
Average	0.004	0.005	0.005	0.005

Table 5-13. Average diametric difference between hole "1" and hole "2"

Donor	Machined	BioCleanse™	Lyophilization	Rehydrated
1	-0.002	0.000	0.003	0.002
2	-0.003	-0.002	-0.003	-0.003
3	-0.001	-0.001	-0.002	0.001
4	-0.013	-0.009	-0.009	-0.009
5	0.007	-0.013	-0.002	-0.005
6	0.000	-0.004	-0.005	-0.003
7	-0.002	-0.004	-0.002	-0.002
8	0.002	0.001	0.003	0.002
9	0.000	0.000	0.000	-0.001
10	-0.003	0.000	0.001	0.000
Max	0.007	0.001	0.003	0.002
Min	-0.013	-0.013	-0.009	-0.009
Range	0.021	0.014	0.012	0.010
St. Dev.	0.005	0.005	0.004	0.003
Average	-0.002	-0.003	-0.002	-0.002

Table 5-14. Average diametric difference in mm between the holes of the two cortical plates of a single allograft.

Donor	Machined	BioCleanse™	Lyophilization	Rehydrated
1	-0.020	0.005	0.001	0.003
2	0.001	0.003	0.004	0.003
3	0.003	0.005	0.006	0.003
4	0.002	0.008	0.012	0.005
5	-0.013	0.016	0.012	0.005
6	0.002	-0.002	-0.002	0.000
7	0.014	-0.006	-0.009	-0.005
8	-0.003	0.002	0.003	0.002
9	0.000	-0.001	0.001	0.000
10	-0.011	-0.006	-0.006	-0.005
Max	0.014	0.016	0.012	0.005
Min	-0.020	-0.006	-0.009	-0.005
Range	0.035	0.022	0.021	0.010
St. Dev.	0.010	0.007	0.007	0.003
Average	-0.003	0.003	0.002	0.001

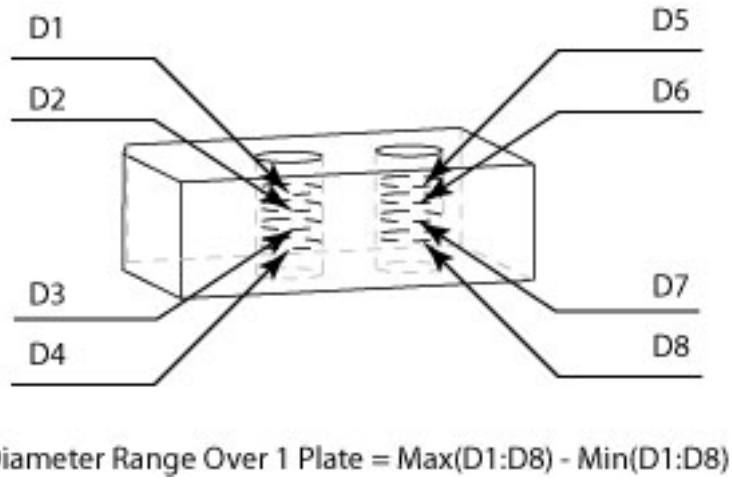

Figure 5-4. Diameter variation over the 8 holes of a single plate.

Table 5-15. Average diameter variation in mm over a single plate.

Donor	Machined	BioCleanse™	Lyophilization	Rehydrated
1	0.018	0.011	0.010	0.010
2	0.007	0.009	0.011	0.010
3	0.011	0.012	0.013	0.015
4	0.015	0.016	0.016	0.016
5	0.020	0.025	0.016	0.016
6	0.003	0.009	0.012	0.005
7	0.007	0.009	0.011	0.010
8	0.009	0.008	0.008	0.008
9	0.003	0.003	0.004	0.004
10	0.009	0.007	0.007	0.006
Max	0.020	0.025	0.016	0.016
Min	0.003	0.003	0.004	0.004
Range	0.017	0.023	0.013	0.012
St. Dev.	0.006	0.006	0.004	0.004
Average	0.010	0.011	0.011	0.010

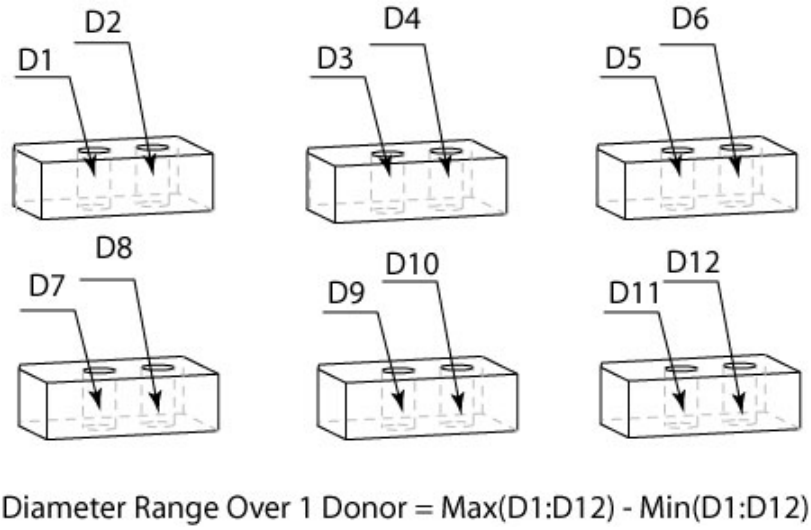

Figure 5-5. Hole diameter variation over all the plates from a given donor.

Table 5-16. Range of hole diameter values in mm over a single donor.

Donor	Machined	BioCleanse™	Lyophilization	Rehydrated
1	0.019	0.016	0.019	0.013
2	0.016	0.017	0.014	0.025
3	0.020	0.022	0.023	0.022
4	0.051	0.039	0.041	0.037
5	0.086	0.063	0.031	0.022
6	0.005	0.016	0.023	0.008
7	0.044	0.037	0.047	0.018
8	0.012	0.009	0.010	0.007
9	0.005	0.005	0.007	0.008
10	0.032	0.011	0.015	0.011
Max	0.086	0.063	0.047	0.037
Min	0.005	0.005	0.007	0.007
Range	0.082	0.057	0.040	0.030
St. Dev.	0.025	0.018	0.013	0.010
Average	0.029	0.024	0.023	0.017

Table 5-17. Average predicted diametric interference in mm for each manufacturing cycle.

Donor	Machined	BioCleanse	Lyophilization	Rehydrated
1	0.045	0.031	0.007	0.024
2	0.043	0.042	0.012	0.033
3	0.028	0.032	0.002	0.004
4	0.033	0.028	0.012	0.021
5	0.048	0.030	0.017	0.021
6	0.030	0.034	0.019	0.019
7	0.035	0.036	0.028	0.030
8	0.029	0.026	0.011	0.024
9	0.019	0.026	-0.006	0.004
10	0.037	0.032	0.011	0.001
Max	0.048	0.042	0.028	0.033
Min	0.019	0.026	-0.006	0.001
Range	0.029	0.016	0.034	0.032
Std Dev	0.009	0.005	0.009	0.011
Average	0.035	0.032	0.011	0.018

Table 5-18. Pull-apart test results

Graft	Manual Pull-apart	Separated Plate	Epoxy	Peak Load (N)	Comments
1-1	No	NA	Quick-setting	82.5	Epoxy failed
2-1	No	NA	Quick-setting	55.8	Epoxy failed
3-1	No	NA	Quick-setting	68.6	Plate broke and separated
1-2	No	NA	Quick-setting	152.3	Epoxy failed
2-2	No	Top	Quick-setting	69.1	Interference fit failed, opposite plate cracked
3-2	Yes	NA	Quick-setting	15.3	Epoxy failed, both plates cracked
1-3	No	Top	Quick-setting	73.5	Interference fit failed
2-3	No	NA	Quick-setting	62.2	Epoxy failed
3-3	No	Bottom	Quick-setting	96.7	Interference fit failed
1-4	No	Top	Quick-setting	93.6	Interference fit failed, opposite plate cracked
2-4	No	Top	Quick-setting	82.4	Interference fit failed
3-4	Yes	Bottom	Quick-setting	61.9	Interference fit failed, removed plate cracked
1-5	No	NA	Quick-setting	114.6	Epoxy failed, one plate cracked
2-5	No	NA	Quick-setting	67.2	Epoxy failed, one plate cracked
3-5	No	NA	Quick-setting	71.7	Epoxy failed, one plate cracked
1-6	No	NA	Quick-setting	64.7	Epoxy failed, one plate cracked
2-6	No	Top	Quick-setting	67.6	Interference fit failed, both plates cracked
3-6	Yes	Top	Metal/Concrete	57.8	Interference fit failed, removed plate cracked
1-7	No	NA	Metal/Concrete	99.5	Epoxy failed
2-7	No	Bottom	Metal/Concrete	71.1	Interference fit failed, both plates cracked
3-7	No	Bottom	Metal/Concrete	94.2	Interference fit failed, opposite plate cracked
1-8	No	Top	Metal/Concrete	118.3	Interference fit failed, removed plate cracked
2-8	No	Top	Metal/Concrete	130.9	Interference fit failed
3-8	No	Top	Metal/Concrete	101.7	Interference fit failed
1-9	No	Top	Metal/Concrete	146.3	Interference fit failed
2-9	No	Bottom	Metal/Concrete	72.5	Interference fit failed
3-9	No	Top	Metal/Concrete	92.4	Interference fit failed, both plates cracked
1-10	No	Bottom	Metal/Concrete	67.0	Interference fit failed, both plates cracked
2-10	No	Top	Metal/Concrete	52.2	Interference fit failed, both plates cracked
3-10	Yes	Top	Metal/Concrete	49.6	Interference fit failed, both plates cracked, opposite plate removed as from manual test

Table 5-19. Pull- apart test results for grafts where the interference fit failed.

Graft	Manual Pull-apart	Predicted Interference (mm)	Interference Adjusted for Lyophilization (mm)	Predicted Interference Adjusted for Hydration (mm)	Peak Load (N)
3-1	No	0.065	0.027	0.045	68.6
2-2	No	0.046	0.015	0.036	69.1
1-3	No	0.059	0.034	0.035	73.5
3-3	No	0.084	0.059	0.060	96.7
1-4	No	0.031	0.011	0.020	93.6
2-4	No	0.044	0.024	0.033	82.4
3-4	Yes	0.037	0.017	0.026	61.9
2-6	No	0.035	0.023	0.023	67.6
3-6	Yes	0.042	0.030	0.030	57.8
2-7	No	0.027	0.020	0.022	71.1
3-7	No	0.042	0.035	0.037	94.2
1-8	No	0.037	0.020	0.032	118.3
2-8	No	0.044	0.027	0.039	130.9
3-8	No	0.030	0.013	0.025	101.7
1-9	No	0.037	0.012	0.022	146.3
2-9	No	0.028	0.003	0.013	72.5
3-9	No	0.015	-0.010	-0.010	92.4
1-10	No	0.038	0.011	0.002	67.0
2-10	No	0.052	0.025	0.016	52.2
3-10	Yes	0.044	0.017	0.008	49.6
				Max	146.3
				Min	49.6
				Std Dev	25.9
				Quick-set Epoxy Avg	76.7
				Metal Epoxy Avg	87.8
				Total Avg	83.4

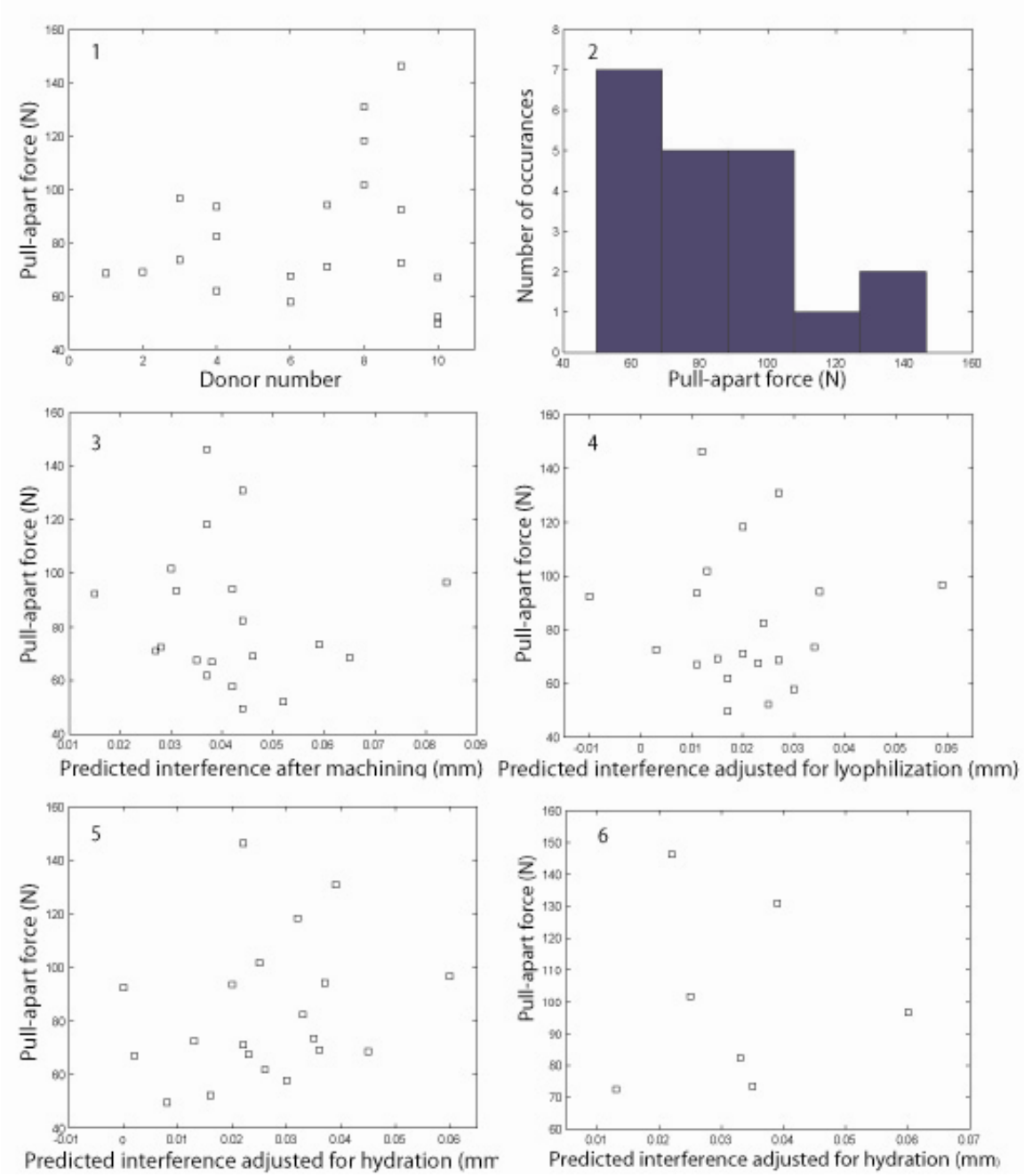

Figure 5-6. Pull-apart test result trends where the interference fit failed. 1) Test results by donor 2) Histogram of the pull-apart forces 3) Pull-apart force vs. predicted interference after machining. 4) Pull-apart force vs. predicted interference adjusted for lyophilization. 5) Pull-apart force vs. predicted interference adjusted for 30 s hydration. 6) Pull-apart force vs. predicted interference adjusted for 30 s hydration: grafts without cracking only.

Table 5-20. Finite element analysis inputs.

Trial	1	2	3
E_r	12.0	12.0	9.0
E_c	12.0	12.0	9.0
E_l	18.0	18.0	14.0
G_{rc}	3.3	3.3	2.9
G_{rl}	3.3	3.3	2.9
G_{cl}	3.3	3.3	2.9
ν_{rc}	0.50	0.50	0.5
ν_{rl}	0.40	0.40	0.4
ν_{cl}	0.25	0.25	0.25
μ	0.29	0.29	0.29
Pin D	1.948	1.936	1.936
Diametric Interference (mm)	0.018	0.011	0.011

Table 5-21. Finite element outputs

Trial	σ_{vm}(max) (Mpa)	Ff (N)
1	80.6	216.0
2	45.0	120.3
3	34.6	93.9

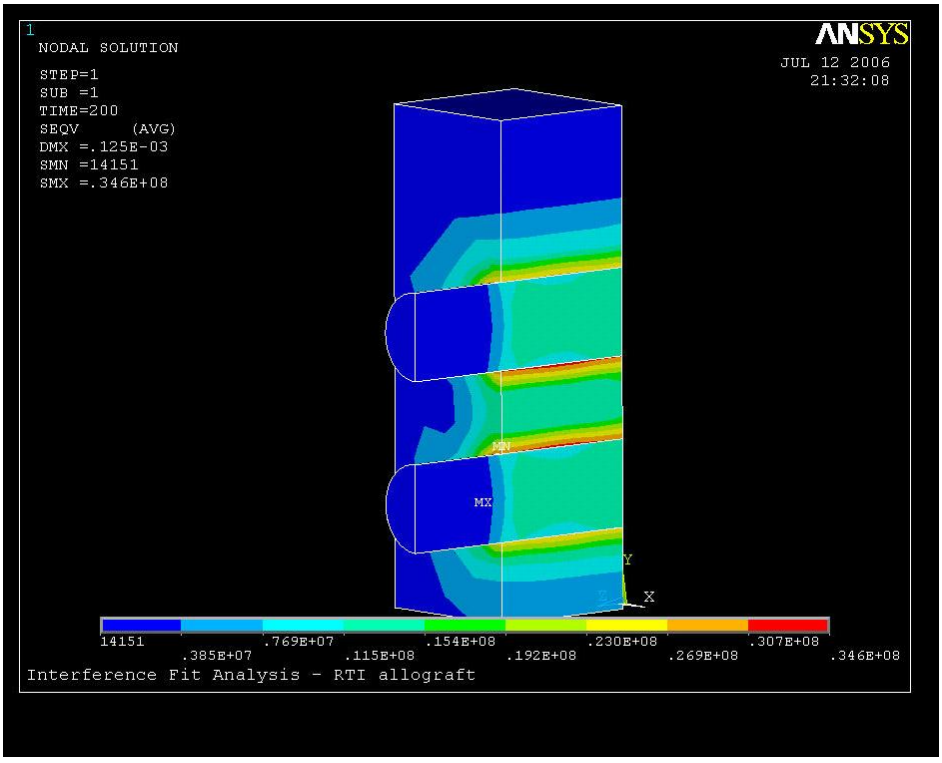

Figure 5-7. Trial 3 von Mises stress distribution

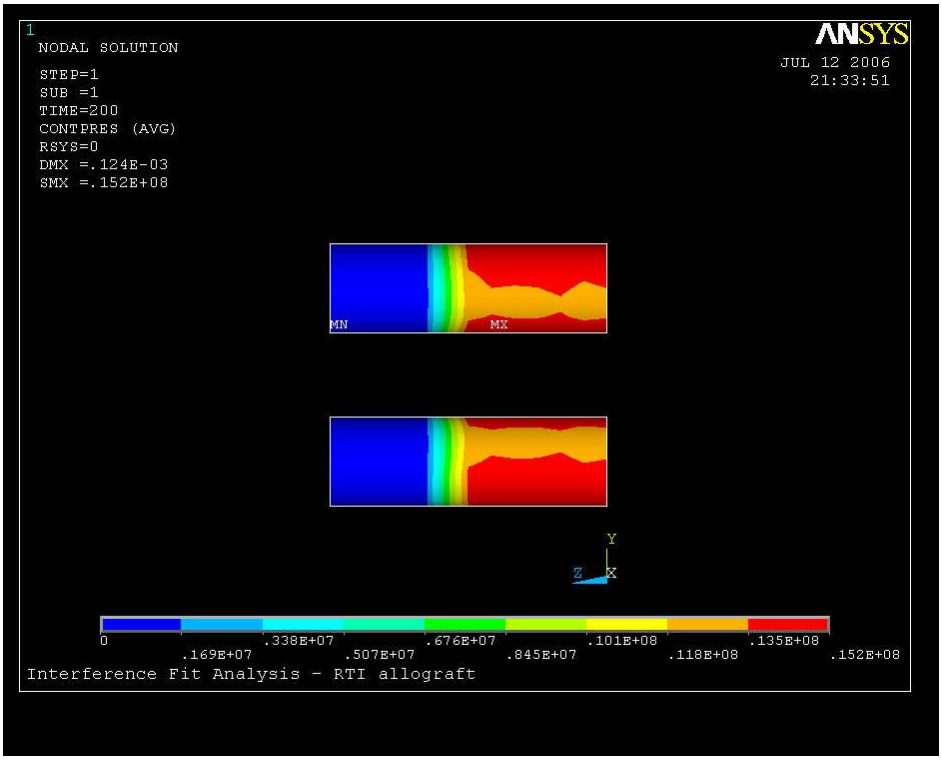

Figure 5-8. Trial 3 pin contact pressure distribution

Table 5-22. Monte Carlo simulation inputs

Parameter	Mean Value	Standard Deviation
Diametric interference (μm)	11	9
Pin Young's modulus (GPa)	9	1
Plate Young's modulus (GPa)	9	1
Pin Poisson's ratio	0.41	0.15
Plate Poisson's ratio	0.41	0.15
Pin diameter (mm)	1.937	0.021
Plate outer radius (mm)	1.2	0
Stress concentration factor	1	0
Contact length (mm)	7.0	0.3
Coefficient of friction	0.3	0.15

Table 5-23. Multi-parameter Monte Carlo simulation overall results.

	Mean Value	Standard Deviation
Pull-apart force (N)	133	141
Von Mises stress (pin) (MPa)	13	7
Von Mises stress (plate) (MPa)	65	39

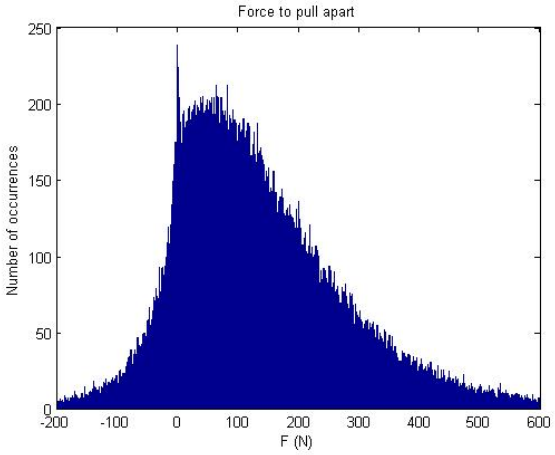

1

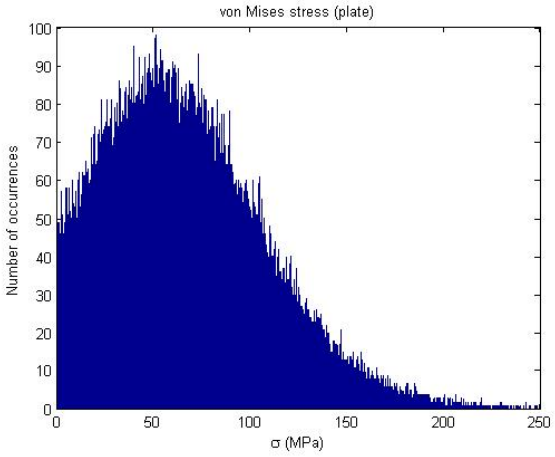

2

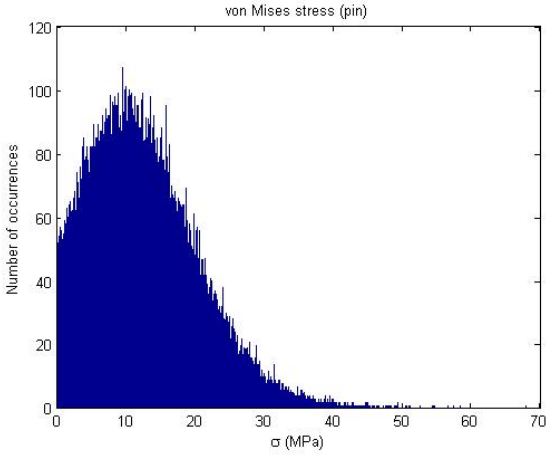

3

Figure 5-9. Monte Carlo simulation results. 1) Pull-apart force. 2) Von Mises stress in the plate. 3) Von Mises stress in the pin.

Table 5-24. Monte Carlo simulation results for single parameter variations

Individual parameters	St. Dev. F (N)	St. Dev. Pin σvm (MPa)	St. Dev. Plt σvm (MPa)
Diametric interference	109	7	38
Coefficient of friction	66	<1	0
Plate Young's modulus	13	1	5
Pin diameter	6	1	1
Contact length	6	1	<1
Pin Poisson's ratio	4	<1	2
Plate Poisson's ratio	4	<1	2

CHAPTER 6
CONCLUSIONS

The diameters of 57 cortical pins from 10 donors were measured. Over a single pin, the average diameter variation was found to be 9 μm with a standard deviation of 3 μm. The average range of pin diameters over single donors was found to be 12 μm after machining, 7 μm after BioCleanse™, 18 μm after lyophilization, and 17 μm after a thirty second hydration.

The hole diameters of 60 cortical plates from 10 donors were measured. The average diameter variation over a single plate was found to be 10-11 μm. Over a single donor, the average range of hole diameters was found to be 29 μm after machining, 24 μm after BioCleanse™, 23 μm after lyophilization, and 17 μm after a thirty second hydration.

Lyophilization was found to have the largest effect on feature size. Cortical pin diameters decreased by an average of 50 μm after lyophilization while cortical plate hole diameters decreased by an average of 29 μm. Thirty seconds of immersion in water caused the pins to regain an average of 11 μm of diameter and the plate holes to regain an average of 3 μm of diameter.

Twenty assembled allografts were pulled apart with a mechanical tensile tester. The average force required to separate the interference fit was 83.4 N with a standard deviation of 25.9 N. Of the allografts without cracked cortical plates, the average pull-apart force was 100.6 N with a standard deviation of 28.5 N. Of the allografts with

cracked cortical plates, the average pull-apart force was found to be 74.1 N with a standard deviation of 19.8 N.

13% of the assembled allografts failed a manual pull-apart test. 57% of the assembled allografts showed signs of cracking.

The sample size of allografts that were not cracked and were successfully pulled apart is too small to derive a correlation between the predicted diametric interference and the pull-apart force. Furthermore, any such correlation may be obscured by variations in donor material properties.

A finite element model was created to model the interference fit. Average geometric conditions from after lyophilization were used while material properties were drawn from the literature. The maximum von Mises stress in the graft was found to be between 34.6 MPa and 80.6 MPa. The pull-apart force required to separate the graft was found to be between 94 N and 216 N.

An analytical model of the interference fit was used to create a Monte Carlo simulation. A Monte Carlo simulation predicted diametric interference, the coefficient of friction, and the plate modulus to be the most influential factors on the interference fit pull-apart force. The simulation predicted diametric interference and elastic properties to be the most influential factors affecting the state of stress in the cortical plates.

The Monte Carlo simulation accurately reflected the frequency of occurrence of pull-apart and cracking failures at 13% and 57%, respectively. The simulation predicted the average pull-apart force to be 133 N with a standard deviation of 141 N and the average von Mises stress in the plate to be 65 MPa with a standard deviation of 39 MPa.

APPENDIX
APPENDIX – MONTE CARLO SIMULATION MATLAB CODE

```
clear all
close all
clc

n = 25e4;                % number of Monte Carlo iterations

% Define variables
mean_delta1 = 11e-6;     % diametral interference (m)
std_delta1 = 9e-6;
delta1 = mean_delta1 + std_delta1*randn(n, 1);
delta = delta1/2;        % radial interference   (m)

mean_Ei = 9E9;           % pin modulus (N/m^2)
std_Ei = 1e9;
Ei = mean_Ei + std_Ei*randn(n, 1);

mean_Eo = 9E9;           % plate modulus (N/m^2)
std_Eo = 1e9;
Eo = mean_Eo + std_Eo*randn(n, 1);

mean_mui = 0.41;         % pin Poisson's ratio
std_mui = 0.15;
mui = mean_mui + std_mui*randn(n, 1);

mean_muo = 0.41;         % plate Poisson's ratio
std_muo = 0.15;
muo = mean_muo + std_muo*randn(n, 1);

mean_b1 = 1.937e-3;           % pin outer diameter (m)
std_b1 = 0.021e-3;
b1 = mean_b1 + std_b1*randn(n, 1);
b = b1/2;                      % pin outer radius

mean_c = 1.2e-3;         % plate outer radius (m)
std_c = 0;
c = mean_c + std_c*randn(n, 1);

mean_Kt = 1;           % stress concentration factor
std_Kt = 0;
Kt = mean_Kt + std_Kt*randn(n, 1);

mean_L = 7e-3;          % axial contact length between pin and plate (m)
std_L = 0.3e-3;            % Note: doubled L to account for 2 pins
```

```
L = mean_L + std_L*randn(n, 1);

mean_cof = 0.3;          % coefficient of friction
std_cof = 0.15;
cof = mean_cof + std_cof*randn(n, 1);

sigma_fail = 25e6;       % Failure stress of bone

%%%%%%%%%%%%%%%%%%%%%%%%%%%%%%%%%%%%%%%%%%%%%%%%%%%%%%%%%%%%%%%%%%%%%%%%%%%%
% Determine pressure, p (N/m^2)
C = b./Eo.*((c.^2 + b.^2)./(c.^2 - b.^2) - muo) + b./Ei.*(1 - mui);
p = delta./C;

% Calculate stresses
sigma_r_i = -Kt.*p;      % pin radial stress (N/m^2)
sigma_t_i = -p;          % pin tangential stress (N/m^2)
sigma_r_o = -Kt.*p;      % plate radial stress (N/m^2)
sigma_t_o = p.*(c.^2 + b.^2)./(c.^2 - b.^2);    % plate tangential
stress (N/m^2)

% pull apart force (N)
F = -2*pi*L.*b.*sigma_r_i.*cof;

% Find all force values greater than zero
Pos_Force = find(F>0);


% Calculate the von Mises stress only for instances where F>0
sigma_p_i = (sigma_r_i(Pos_Force).^2 -
sigma_r_i(Pos_Force).*sigma_t_i(Pos_Force) +
sigma_t_i(Pos_Force).^2).^0.5;% pin
sigma_p_o = (sigma_r_o(Pos_Force).^2 -
sigma_r_o(Pos_Force).*sigma_t_o(Pos_Force) +
sigma_t_o(Pos_Force).^2).^0.5;% plate


%Calculate some statistical parameters
Fmean = mean(F)
Fstd = std(F)
PercFLessZero = length(find(F<0))/n*100
Sigmapin = mean(sigma_p_i)
StdSigmapin = std(sigma_p_i)
PercSMoreFail2 =
length(find(sigma_p_i>sigma_fail))/length(Pos_Force)*100
Sigmaplate = mean(sigma_p_o)
StdSigmaplate = std(sigma_p_o)
PercSMoreFail =
length(find(sigma_p_o>sigma_fail))/length(Pos_Force)*100

bins = 10000;
figure(1)
hist(sigma_p_i/1e6, bins)
xlabel('\sigma (MPa)')
ylabel('Number of occurrences')
title('von Mises stress (pin)')
```

```
set(gcf,'color','white')
 xlim([0 70])

figure(2)
hist(sigma_p_o/1e6, bins)
xlabel('\sigma (MPa)')
ylabel('Number of occurrences')
title('von Mises stress (plate)')
set(gcf,'color','white')
xlim([0 250])

figure(3)
hist(F, bins)
xlabel('F (N)')
ylabel('Number of occurrences')
title('Force to pull apart')
xlim([-200,600])
     set(gcf,'color','white')
```

LIST OF REFERENCES

1. Cowin, S. (1989). *Bone Mechanics*. CRC Press, Inc., Boca Raton, FL.

2. Rho, J., L. Kuhn-Spearing, P. Zioupos (1998). "Mechanical properties and the hierarchical structure of bone." *Medical Engineering and Physics*. 20(2): 92-102.

3. Currey, J. (2002). *Bones: Structure and Mechanics.* Princeton University Press, Princeton, NJ.

4. Huiskes, R. (1982). "On the modeling of long bones in structural analyses." *Journal of Biomechanics* 15(1): 65-69.

5. Bianchi, J. (1999). *Design and Mechanical Behavior of the MD Series of Bone dowels*. University of Florida, Gainesville, FL. Doctor of Philosophy.

6. Choi, K., J. Kuhn, M. Ciarelli, S. Goldstein (1990). The elastic moduli of human subchondral, trabecular, and cortical bone tissue and the size depencency of cortical bone modulus." *Journal of Biomechanics* 23(11): 1103-1113.

7. Zioupos, P., J. Currey (1998). "Changes in the stiffness, strength, and toughness of human cortical bone with age." *Bone* 22(1): 57-66.

8. Akkus, O., F. Adar, M. Schaffler (2004). "Age related changes in physiochemical properties of mineral crystals are related to impared mechanical function of cortical bone." *Bone* 34(3): 443-453.

9. Bensamoun, S., M. Tho, S. Luu, J. Gherbezza, J. de Belleval (2004). "Spatial distribution of acoustic and elastic properties of human femoral cortical bone." *Journal of Biomechanics* 37(4): 503-510.

10. Dunham, C., S. Takaki, J. Johnson, C. Dunning (2005). "Mechanical properties of cancellous bone of the distal humerus." *Clinical Biomechanics* 20(8): 834-838.

11. Hoc, T., L. Henry, M. Verdier, D. Aubry, L. Sedel, A. Meunier (2006). "Effect of microstructure on the mechanical properties of haversian cortical bone." *Bone* 38(4) 466-474.

12. Lotz, J., T. Gerhart, W. Hayes (1990). "Mechanical properties of trabecular bone from the proximal femur – a quantitative CT study." *Journal of Computer Assisted Tomography* 14(1) 107-114.

13. Dalstra, M., R. Huiskes, A. Odgaard, L. Vanerning (1993). "Mechanical and textural properties of pelvic trabecular bone." *Journal of Biomechanics* 26(4-5): 523-535.

14. Rho, J., M. Roy, T. Tsui, G. Pharr (1999). "Elastic properties of microstructural components of human bone tissue as measured by nanoindentation." *Journal of Biomedical Materials Research* 45(1): 48-54.

15. Bensamoun, S., J. Gherbezza, J. de Belleval, M. Tho (2004). "Transmission scanning acoustic imaging of human cortical bone and relation with the microstructure." *Clinical Biomechanics* 19(6): 639-647.

16. Reilly, D. and A. Burstein (1975). "The elastic modulus and ultimate properties of compact bone tissue." *Journal of Biomechanics* 8: 393.

17. Yoon, H. and J. Katz (1976). "Ultrasonic wave propagation in human cortical bone II: Measurements of elastic properties and micro-hardness." *Journal of Biomechanis* 9: 459.

18. Knets, I. and A. Malmeisters (1977). "Deformability and strength of human compact bone tissue." Proceedings of the Euromech Colloquium on Mechanics of Biological Solids. 133. Ed. G. Brankov. Bulgarian Academy of Sciences, Sofia, Bulgaria.

19. Ashman, R., S. Cowin, W. Van Buskirk, J. Rice (1984). "A continuous wave technique for the measurement of the elastic properties of cortical bone." *Journal of Biomechanics* 17: 349-361.

20. Kabel, J., B. van Rietbergen, M. Dalstra, A. Odgaard, R. Huiskes (1999). "The role of an effective isotropic tissue modulus in the elastic properties of cancellous bone." *Journal of Biomechanics* 32(7): 673-680.

21. Rice, J., S. Cowin, J. Bowman (1988). "On the dependency of the elasticity and strength of cancellous bone on apparent density." *Journal of Biomechanics* 21(2): 155-178.

22. Shigley, J. and C. Mischke (2001). *Mechanical Engineering Design*. McGraw-Hill, New York, New York.

23. Nagasao, T., M. Kobayashi, Y. Tsuchiya, T. Kaneko, T. Nakajima (2002). "Finite element analysis of the stresses around endosseous implants in various reconstructed mandibular models. *Journal of Cranio-Maxillofacial Surgery* 30(3): 170-177.

24. Nagasao, T., M. Kobayashi, Y. Tsuchiya, T. Kaneko, T. Nakajima (2002). "Finite element analysis of the stresses around fixtures in various reconstructed mandibular models – Part II (effect of horizontal load). *Journal of Cranio-Maxillofacial Surgery* 31(3): 168-175.

25. Tie, Y., D. Wang, C. Wang, C. Zhang (2006). "Three-dimensional finite-element analysis investigating the biomechanical effects of human mandibular reconstruction with autogenous bone grafts." *Journal of Cranio-Maxifillofacial Surgery – Article in press.*

26. Barker, D., D. Netherway, J. Krishnan, T. Hearn (2005). "Validation of a finite element model of the human metacarpal." *Medical Engineering & Physics* 27(2): 103-113.

27. Wang, X., G. Dumas (2005). "Evaluation of effects of selected factors on inter-vertebral fusion – a simulation study." *Medical Engineering & Physics* 27 (3): 197-207.

28. Zapata, J. (2001). Reduction of stress concentration around a surgically drilled hole in cortical bone. University of Florida, Gainesville, FL. Master of Science.

29. Yew, D. "Virtual anatomy" http://www.ana.cuhk.edu.hk/3dana/main.htm. Last accessed July 2, 2006.

30. Mroz, T., E. Lin, M. Summit, J. Bianchi, J. Keesling, M. Roberts, C. Vangsness, J. Wang (2006). "Biomechanical analysis of allograft bone treated with a novel tissue sterilization process." *The Spine Journal* 6: 34-39.

31. American National Standard ASME B89.4.1-2001b. New York, NY.

BIOGRAPHICAL SKETCH

Nate Mauntler was born on April 10, 1981, the second of four sons of John and Margaret Mauntler. He graduated from Troy High School in Troy, Ohio, in June of 1999. Mr. Mauntler then left Ohio to pursue a Bachelor of Science degree in mechanical engineering at the University of Florida, which was completed in May of 2004. Since that time, Mr. Mauntler has been continuing his education at the University of Florida in pursuit of a master's degree in mechanical engineering. This thesis was written in partial fulfillment of this degree. Upon graduation, Mr. Mauntler will stay on at the University of Florida Tribology Laboratory and Machine Tool Research Center to pursue a doctoral degree.